ACSNANO

www.acsnano.org

ARTICLE

A Bioactive Disintegrable Polymer Nanoparticle for Synergistic Vascular Anticalcification

Hossein Adelnia, Shehzahdi Shebbrin Moonshi, Yuao Wu, Andrew C. Bulmer, Ryan Mckinnon, Jarred William Fastier-Wooller, Idriss Blakey, and Hang Thu Ta*

Cite This: *ACS Nano* 2023, 17, 18775–18791

Read Online

ACCESS | Metrics & More | Article Recommendations | Supporting Information

ABSTRACT: **Although poly(aspartic acid) (PASP), a strong calcium chelating agent, may be potentially effective in inhibition of vascular calcification, its direct administration may lead to side effects. In this study, we employed polysuccinimide, a precursor of PASP, to prepare targeted polysuccinimide-based nanoparticles (PSI NPs) that not only acted as a prodrug but also functioned as a carrier of additional therapeutics to provide powerful synergistic vascular anticalcification effect. This paper shows that chemically modified PSI-NPs can serve as effective nanocarriers for loading of hydrophobic drugs, in addition to anticalcification and antireactive oxygen species (anti-ROS) activities. Curcumin (Cur), with high loading efficiency, was encapsulated into the NPs. The NPs were stable for 16 h in physiological conditions and then slowly dissolved/hydrolyzed to release the therapeutic PASP and the encapsulated drug. The drug release profile was found to be in good agreement with the NP dissolution profile such that complete release occurred after 48 h at physiological conditions. However, under acidic conditions, the NPs were stable, and Cur cumulative release reached only 30% after 1 week. Though highly effective in the prevention of calcium deposition, PSI NPs could not prevent the osteogenic trans-differentiation of vascular smooth muscle cells (VSMCs). The presence of Cur addressed this problem. It not only further reduced ROS level in macrophages but also prevented osteogenic differentiation of VSMCs *in vitro*. The NPs were examined *in vivo* in a rat model of vascular calcification induced by kidney failure through an adenine diet. The inclusion of Cur and PSI NPs combined the therapeutic effects of both. Cur-loaded NPs significantly reduced calcium deposition in the aorta without adversely affecting bone integrity or noticeable side effects/toxicity as examined by organ histological and serum biochemistry analyses.**

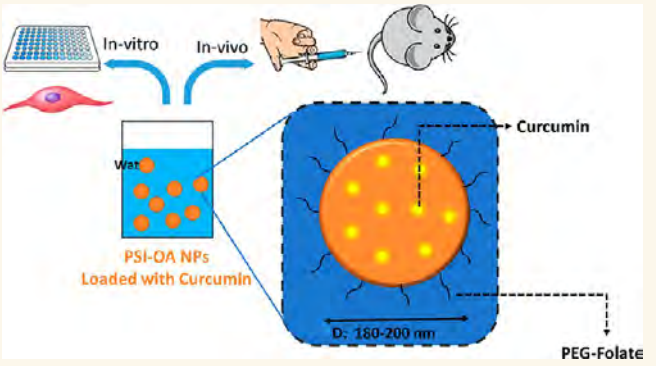

KEYWORDS: *polysuccinimide, curcumin, anticalcification, antioxidant, vascular calcification, chronic kidney disease*

INTRODUCTION

Vascular calcification can lead to stiffening of the vasculature, hypertension, stenosis, and a range of other adverse cardiovascular changes, resulting in a high rate of mortality.[1−3] Vascular calcification is markedly accelerated in patients with chronic kidney disease and is associated with higher patient mortality.[1,4] During this process, calcium phosphate crystallizes in the form of hydroxyapatite, predominately depositing in vascular smooth muscle tissues, the valves, and aorta.[5] Calcification can occur in either the medial or the intimal layers of the arterial wall. Intimal calcification is associated with atherosclerosis, whereas medial calcification occurs along the degraded elastin fibers around smooth muscle cells and is mainly related to chronic kidney disease. Medial calcification causes loss of vessel elasticity, resulting in increased systolic blood pressure and left ventricle hypertrophy which may ultimately lead to arrhythmia and heart failure.[6] To date, no clinically viable therapies for the treatment and prevention of vascular calcification have been approved.[7] As such, an early and effective treatment for vascular calcification related to chronic kidney disease is urgently needed.

Received: April 4, 2023
Accepted: August 23, 2023
Published: August 31, 2023

Scheme 1. Schematic Representation of Structure of Oleylamine-Modified Poly(succinimide) Nanoparticles (PSI-OA NPs) Loaded with Curcumin and Conjugated with Folic Acid-PEG

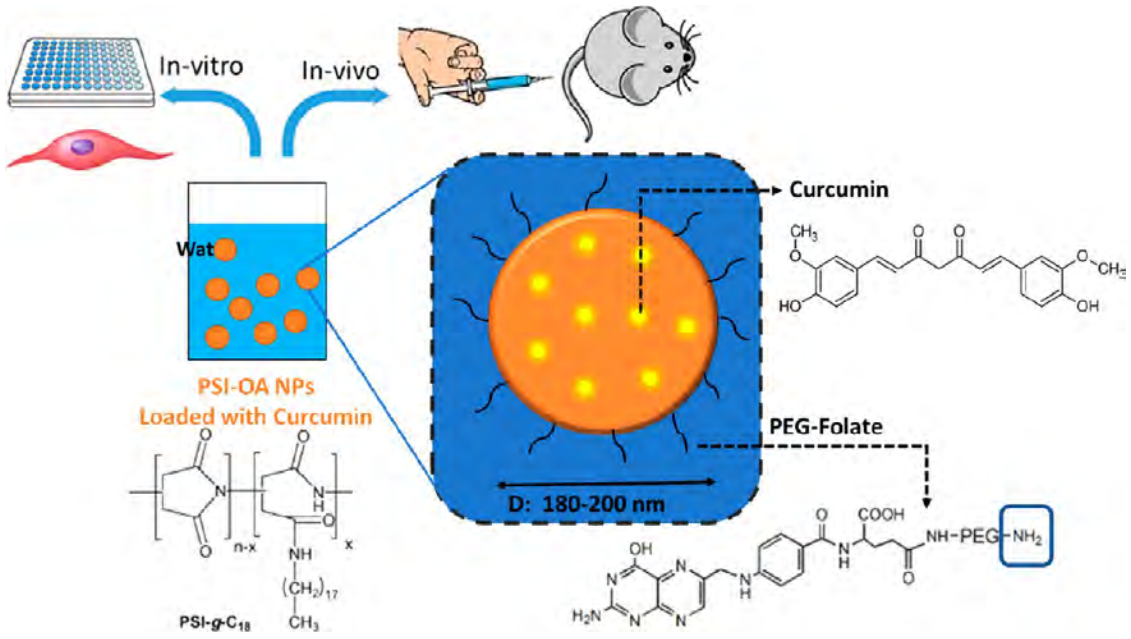

While metal ions such as calcium, copper, and iron are critical for life, their surplus can lead to detrimental impacts to cells, tissues, and organs mainly through generation of reactive oxygen species (ROS).[8] Excess ROS has emerged as a significant contributor in many chronic diseases.[9−13] For example, high levels of calcium and iron have been correlated to vascular calcification and cancer, respectively.[14,15] Sequestration of these ions via application of an appropriate complexing agent, referred to as chelator, has been widely adopted as a potential treatment strategy. Iron and copper in the complexed forms are not active in catalyzing the ROS generation reaction via the Fenton and Haber−Weiss reactions. Likewise, hypercalcemia leads to calcium deposition only if calcium is not bound.

Poly(aspartic acid) (PASP) and its derivatives are strong polypeptide-based chelating agents for different metal ions and have been exploited in a variety of areas.[16,17] However, despite simple synthesizability, modifiability, biocompatibility, and biodegradability, their biomedical applications have not been explored very well. We recently reviewed the chelation abilities of PASP and the potential it can offer in biomedical applications.[18] PASP was highly efficacious in reducing the toxicity and thus mortality in zebrafish induced by heavy metal ions.[19] PASP-based polymers have also reduced the toxicity of iron-oxide NPs as reported in different studies, due to iron chelation.[20] Several works have also confirmed the effectiveness of PASP in the inhibition and even dissolution of calcium oxalate monohydrate, the main mineral of kidney stones.[21−24]

Overall, chelation therapy based on PASP could potentially be a viable approach for lowering the ROS and treating vascular calcification. However, due to hydrophilicity, PASP can chelate ions once administered, thereby dropping the level of essential ions suddenly. This may lead not only to PASP's ineffectiveness but also to severe side effects, as has been reported in the case of other chelators such as ethylenediaminetetraacetic acid (EDTA). Therefore, in our study we proposed using polysuccinimide (PSI), a precursor of PASP, instead of PASP to avoid potential side-effects associated with the direct administration of PASP. We recently showed that PASP could be spontaneously, inherently, and slowly synthesized in the physiological conditions from its precursor PSI.[25]

In addition to its bioactivity, PSI, as a hydrophobic polymer, can also serve as a carrier of hydrophobic agents, providing a potential platform for the delivery of drugs that are clinically limited with drawbacks, such as low aqueous solubility and rapid metabolism/degradation. Due to the slow conversion to PASP, PSI NPs are expected to release their cargo in a sustained manner, consistent with their dissolution profile. Therefore, in order to enhance the therapeutic efficiency of the formulation, appropriate therapeutic agents could be loaded into the NPs. Several investigations have been conducted on the biodegradability of nanomaterials in a biological milieu, demonstrating promising outcomes for instance in terms of therapeutic efficacy and release profiles (e.g., erosion-based release mechanisms).[26−31] Curcumin (Cur), a natural polyphenolic compound, has been established as a promising drug in a variety of diseases.[32,33] Cur has powerful anti-inflammatory, antioxidant, and anticalcification properties; however, its clinical application is hindered by several drawbacks, including low aqueous solubility and rapid metabolism.[34] Cur loading into PSI NPs not only addresses these limitations but also enables targeting of delivery of Cur to the disease site.

In this study, we strategically combined the chelation effect of PSI and the therapeutic activities of Cur to render a powerful NP for synergistic vascular anticalcification (Scheme 1). PSI NPs were chemically modified to achieve stability for 16 h in physiological conditions, allowing time to reach the disease site where they slowly dissolved to release the therapeutic PASP and the encapsulated Cur. Overall, this study first prepared PSI NPs modified with oleyl amine (OA), conjugated them with different molecules, and investigated loading and release of Cur. The efficacy of the prepared NPs was then evaluated in *in vitro* ROS and calcification experiments. Finally, the NPs were examined in *in vivo* studies

https://doi.org/10.1021/acsnano.3c03041
ACS Nano 2023, 17, 18775−18791

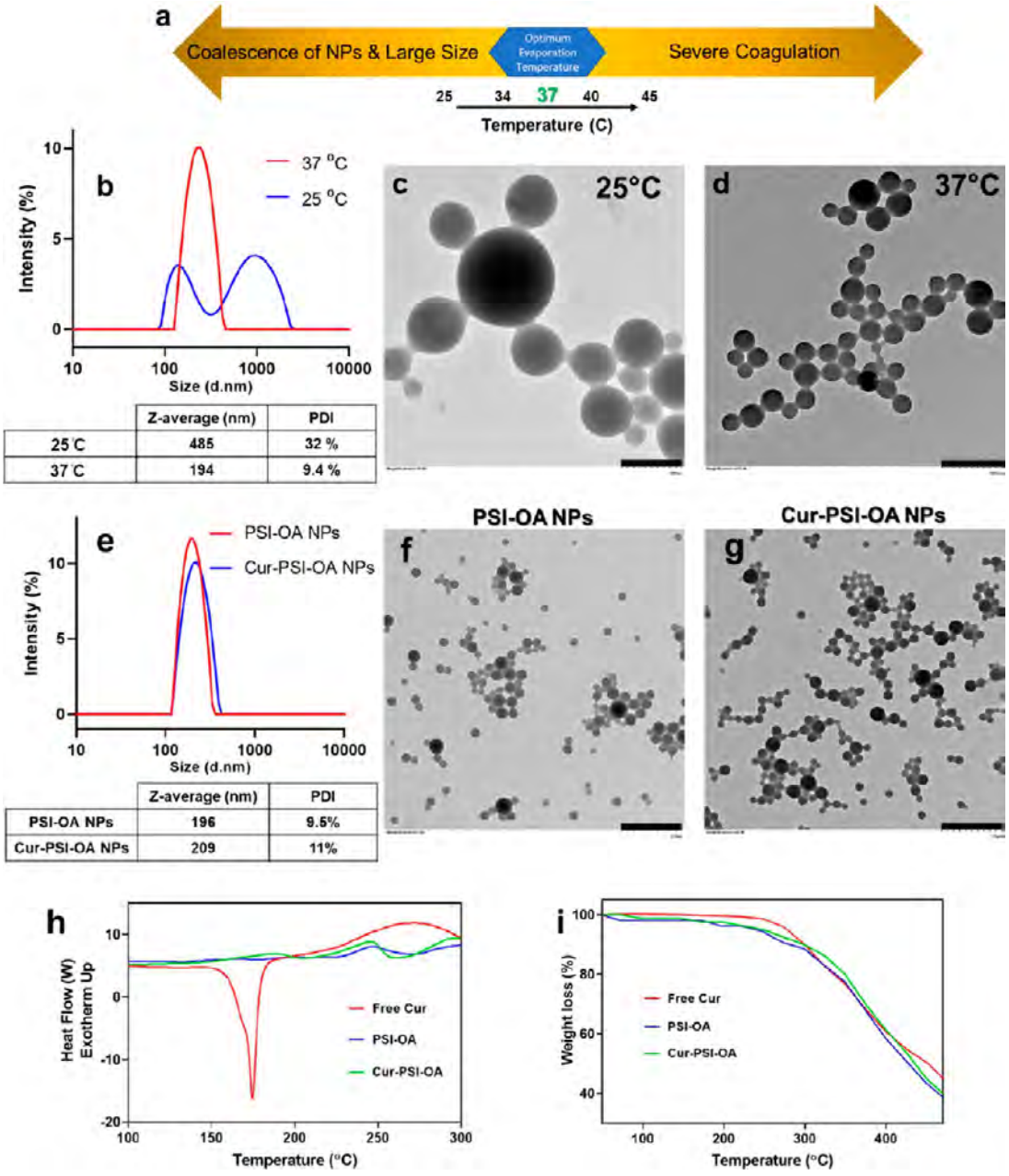

Figure 1. Preparation and optimization of PSI-OA NPs by the emulsion evaporation method. (a) The optimum temperature in the evaporation step was found to be 37 ± 1 °C. (b) Size distribution in terms of intensity percentage obtained by DLS and (c) TEM images of the optimized sample. The optimum condition for the preparation of the NPs requires DCM as the solvent, PSI-OA concentration of 20 mg/mL, fully hydrolyzed PVA (1%) as polymeric stabilizer, and evaporation of DCM at 37 ± 2 °C for at least 2 h. The detailed procedure is presented in the experimental section. The scale bar is 500 nm. (e) DLS, (f and g) TEM, (h) DSC, and (i) TGA results for PSI-OA and Cur-PSI-OA NPs. The NPs were prepared by 2.5 wt % partially hydrolyzed PVA with room-temperature solidification temperature. The scale bar is 1 μm.

on a rat model of vascular calcification induced through kidney failure by an adenine diet.

RESULTS AND DISCUSSION

Synthesis and Characterization of PSI-OA NPs. Synthesis, characterization, and dissolution of PSI NPs have already been presented in our previous paper. It was reported that the precipitation method can yield colloidally stable NPs with a size in the range of 150−500 nm. Nevertheless, loading of hydrophobic agents using the nanoprecipitation method is problematic because the solubility threshold of polymer and the drug could be quite different, leading to the formation of free polymer NPs (i.e., unloaded) and aggregation/crystallization of the hydrophobic agent. Cur loading into the PSI-OA polymer tested by the precipitation method revealed a very low level of loading (up to 2−5%). Conducting the precipitation experiment in the absence of polymer revealed that Cur precipitates much later than the polymer does. Therefore, the emulsion method was adopted for loading of bioactive agents, which will be discussed further below. Characterization of the chemical structure of PSI-OA with FTIR and H NMR is presented in Figure S2.

https://doi.org/10.1021/acsnano.3c03041
ACS Nano 2023, 17, 18775−18791

For the preparation of PSI-OA NPs, several parameters, including solvent, evaporation temperature, and emulsifiers, were tested to obtain small (<250 nm) and stable NPs with narrow particle size distribution (Figure 1a−c). Briefly, it was found that DCM, compared to chloroform as the solvent for the polymer, resulted in a much better colloidal stability. When fully hydrolyzed PVA (1 wt %) was used as the stabilizer, a solidification temperature of 37 °C was found to be optimum. Higher PVA concentrations increased the emulsion viscosity and size. Higher temperatures (e.g., 45 °C) led to an unstable system, severe coagulation, and the formation of large coagulum, which could be attributed to DCM boiling (boiling point, 39.6 °C); thus, DCM boiled quickly, making the emulsion highly unstable. It is noteworthy that the stable part of the sample showed NP rupture and breakage as a result of sudden phase change from liquid to gas for DCM. Slow evaporation of DCM at room temperature, however, was not in favor of the formation of small NPs. This could be due to coalescence of the droplets, as the emulsion is not thermodynamically stable. In other words, prior to the NP formation, droplets slowly merged, thereby increasing the size. At 25 °C, the *z*-average was 485 nm and PDI was 0.32 (Figure 1b,c). Therefore, an optimum temperature is required, which was found to be 37 °C. At this temperature, the NPs had the size of 194 nm with a narrow PDI of 0.094 as seen in the DLS graph and TEM image (Figure 1b,d). Interestingly, when partially hydrolyzed PVA (2.5 wt.%) was used, the NPs were similar size both at 25 and 37 °C, which is due to the stronger stabilizing activity of PVA. (Figure 1e). Although room-temperature incubation overnight yields stable NPs with small size, proper mixing should be carried out to prevent foam formation as air bubbles accumulate on the emulsion surface, retarding DCM evaporation and resulting in coalescence and large NPs. Lower concentrations of partially hydrolyzed PVA did not stabilize the emulsion well.

Cur was loaded into the NPs at 2 different Cur:PSI mass ratios of 1:20 and 1:40. The encapsulation efficiency (%) values of 86 ± 8 and 79 ± 6 were obtained, respectively. Such a high encapsulation efficiency in the emulsion evaporation method compared to that in the precipitation method was attributed to an efficient entrapment of Cur by the polymer. The NP size increased by approximately 15 nm after Cur loading, indicating Cur entrapment inside the NPs. As seen in the DLS results (Figure 1e), colloidally stable NPs with relatively narrow size distribution were obtained. As TEM images (Figure 1f,g) showed, the NPs were spherical shaped, and there was no sign of aggregation or crystallized impurities, which is indicative of unloaded Cur.

The thermal decomposition behavior and kinetics of PSI-OA and Cur-PSI-OA NPs were assessed by TGA and DSC methods. The DSC results (Figure 1h) further confirmed efficient Cur loading into the PSI-OA NPs. The sharp endothermic peak centered at 172 °C for Cur powder was attributed to melting of crystalline Cur. The absence of a Cur melting point peak in PSI-Cur NPs showed that Cur underwent a phase transition from crystalline to amorphous and that the NP formation strongly inhibited Cur crystallization. Amorphous phase was the result of uniform mixing of Cur in PSI-OA under a molecular scale, suggesting the high level of physiochemical compatibility of Cur and PSI-OA due to their hydrophobicity. The TGA results (Figure 1i) show a typical degradation of organic materials, in which Cur, PSI-OA, and Cur-PSA-OA showed an initial weight loss at approximately 280 °C followed by a fast decomposition.

Conjugation of the NPs with Cy5 or Folic-PEG. As discussed above, PSI can be easily modified with a variety of amine-containing molecules (e.g., antibodies, aptamers, dyes, etc.) due to the presence of highly reactive succinimide groups on the NP surface.[17] Therefore, the surface functionalization of the prepared PSI-OA NPs could also be relatively straightforward. In fact, in contrast to carboxylic acid functionality, which requires activation for functionalization through different chemistries such as EDC/NHS, high reactivity of succinimide with amine enables room-temperature, catalyst-free conjugations. Nevertheless, optimization of the conjugation process would be necessary to prevent NP disintegration if the conjugating molecule is highly hydrophilic, and this will be discussed below. Two conjugation experiments were carried out involving Cy5-amine and folic acid-polyethyelene glycol-amine (FA-PEG-NH_2) (Figure S3). The former is a fluorophore, while the latter is used for targeting the cell's overexpressing folic receptor. For the Cy5 conjugation, successful conjugation is obvious as seen in the photographs (Figure S3a). The pellet (i.e., centrifuged NPs) had a blue color. As the concentration of the fluorophore was increased, the supernatant becomes bluish, which indicates the fact that the NP surface has been saturated and no more Cy5 can be attached, thus remaining unreacted in the supernatant. The FL intensity of the supernatant as a function of its initial concentration in the feed also verified such a saturation. Up to 4 μM of Cy5, the FL intensity of the supernatant remained almost constant, while at higher concentrations, it increased linearly (Figure S3a). Therefore, one can conclude that the Cy5 concentration around 4 μM is the maximum level for conjugation of 500 μg/mL PSI-OA, saturating the NP surface. This concentration is equivalent to 8 nmol of Cy5 per 1 mg of PSI-OA NPs or 5.2 μg/mg of PSI-OA NPs.

As shown in Figure S3b,c, PEGylation (surface conjugation by PEG) was confirmed by the presence of the characteristic peak of PEG in the ATR-FTIR of the conjugated NPs (peak at 1088 cm^{-1}). PEGylation is also known to decrease the absolute value of the zeta potentials. The surface charge, regardless of being either positive or negative, is screened and thus reduced by the conjugation of PEG, a nonionic oligomer/polymer. As seen in Table S1, zeta potentials of the NPs decreased from −19 mV to −10 mV when FA-PEG-NH_2 was reacted with the NPs (1:10 mass ratio). A higher concentration of FA-PEG-NH_2 increased the size and increased the absolute value of the zeta potential. Nevertheless, the count rate in the DLS measurement at FA-PEG-NH_2:PSI-OA NPs ratios higher than 1:10 decreased by 1 order of magnitude, suggesting the dissolution and disintegration of the NPs. In fact, hydrophilic FA-PEG-NH_2 chains attached on the PSI-OA surface react with succinimide, forming an amide bond, thereby slowly detaching the PSI-OA chains from the NP surface. This behavior was not observed in the case of Cy5-amine conjugation due to its relative hydrophobicity. Therefore, considering the low count rate density, the measured size at those ratios could not be representative of the actual hard spheres of the polymer. The optimum ratio of FA-PEG-NH_2:PSI-OA was thus concluded to be 1:10 and used for further experiments. Other parameters such as Cur:polymer ratio was set at 1:20 as it yielded high encapsulation efficiency (%) values of 86 ± 8, as mentioned above.

https://doi.org/10.1021/acsnano.3c03041
ACS Nano 2023, 17, 18775−18791

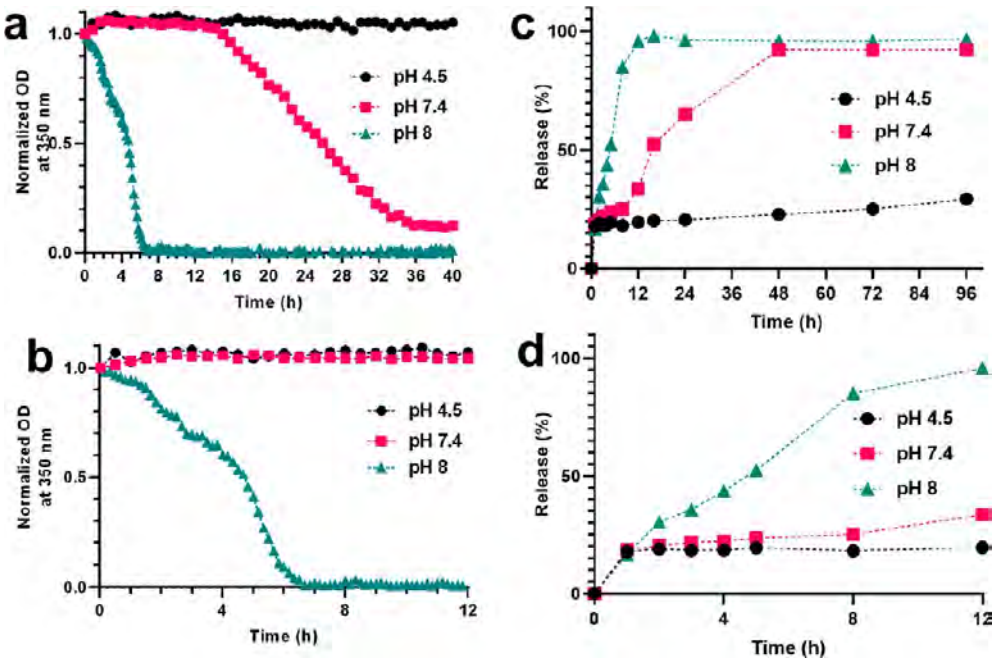

Figure 2. Dissolution of PSI-OA NPs and release of Cur from them. (a) Normalized optical density (at 350 nm) of PSI-OA NPs at 37 °C as a function of time at different media including human plasma, serum, DI water, acetate buffer pH 4.5, as well as PBS with pH 7.4 having different strengths of 1×, 2.5×, 5×, and 10×. (b) The corresponding OD in graph in panel a in the range of 0−12 h. (c) Release of Cur from the NPs at different pH condition with 0.2% tween at 37 °C over 96 h. (d) Magnified part of panel c up to 12 h.

Stability of the NPs at Different Conditions. The prepared NPs were stable at slightly acidic conditions, whereas upon increasing pH, they disintegrated and dissolved in the medium (Figure 2a,b). The dissolution of the NPs is reflected by a decrease in the optical density of the NPs. Constant optical density over time is indicative of colloidal stability. In contrast, the increase in optical density could suggest the increase in size of the NPs as a result of aggregation, since the large-size aggregates have higher turbidity. The dissolution of the NPs is the consequence of hydrolysis of hydrophobic succinimide groups by hydroxide ions (OH^-), yielding a water-soluble aspartic acid residue in the polymer structure. The reason for stability at acidic condition is thus due to a low level of OH^-. Very low pH values (<2), however, adversely affected the colloidal stability of the system. As demonstrated above, the NPs are slightly negatively charged. The negative charge stems from either the functional groups at the end of the PSI chains (i.e., aspartic acid), or partial hydrolysis of succinimide groups on the NP surface, again leaving aspartic acid behind. The negatively charged colloids are typically unstable under acidic media, as the acidic groups (carboxylic acid groups in this case) become protonated, thereby reducing the surface charge density and charge repulsion, which in turn leads to aggregation and coagulation. Of note is that the PSI-OA NPs have a relatively long stability (around 10 h) in PBS at 37 °C (Figure 2b). This is in contrast to the fast dissolution of pure PSI NPs shown in our previous study, where their dissolution commenced from the beginning of the incubation. The stability of the PSI-OA could be attributed to the presence of highly hydrophobic oleyl amine grafted on the polymer backbone, making the NPs hydrophobic, creating steric hindrance for water diffusion, and delaying the onset of dissolution. Overall, such a dissolution profile could potentially be exploited for the targeted delivery and sustained release of a variety of hydrophobic agents through polymer dissolution/hydrolysis (i.e., erosion release mechanism). Future studies will utilize TEM for cross-validation of the absorbance reduction in different media.

The release of Cur from the NPs was evaluated quantitatively in different media containing 0.2 wt % Tween 80, pH values of 4.5, 7.4, and 8 at 37 °C for 96 h (Figure 2c,d). As can be seen, the release profile at pH 8 is much faster than that in pH 7.4. At pH 7.4, there was a plateau at first 12 h with a very small amount of Cur released. This was followed by a quick release afterward and the completion of release after 2 days, where the dispersions turned completely transparent yellow. The release at pH 4.5 was very slow and remained at approximately 30% after 1 week. Overall, these release profiles are in a good agreement with the NP dissolution profile where at pH 7.4 and 8 no NPs existed after 35 and 20 h, respectively, as they are converted to water-soluble PASP-OA. Such a release profile could have potential for designing oral delivery systems as well as the treatment of colon-related disease and thus present PSI-OA NPs as a potential alternative for Eudragit which is a nondegradable acrylic-based polymer currently used for oral administration drug delivery.[35−37] In fact, owing to the stability at acidic pH conditions, the NPs can remain stable in the acidic conditions of the stomach, protecting the susceptible/degradable cargo. After passing through the stomach, as the pH increases, the particles slowly dissolve and release the payload in the small intestine and colon.

Viability and Uptake Study of Macrophage RAW Cells. Biocompatibility of PSI-OA NPs with RAW cells and MOVAS was investigated, which are shown in Figure 3a,b and Figure S4, respectively. The NPs did not pose any noticeable toxicity to RAW cells for 2 days and to MOVAS for 3 days at the concentrations tested. The biocompatibility of PASP-OA as the hydrolysis product of PSI-OA NP was also tested, which similarly showed no noticeable toxicity. These results are in agreement with those of the literature, where PASP and PSI

https://doi.org/10.1021/acsnano.3c03041
ACS Nano 2023, 17, 18775−18791

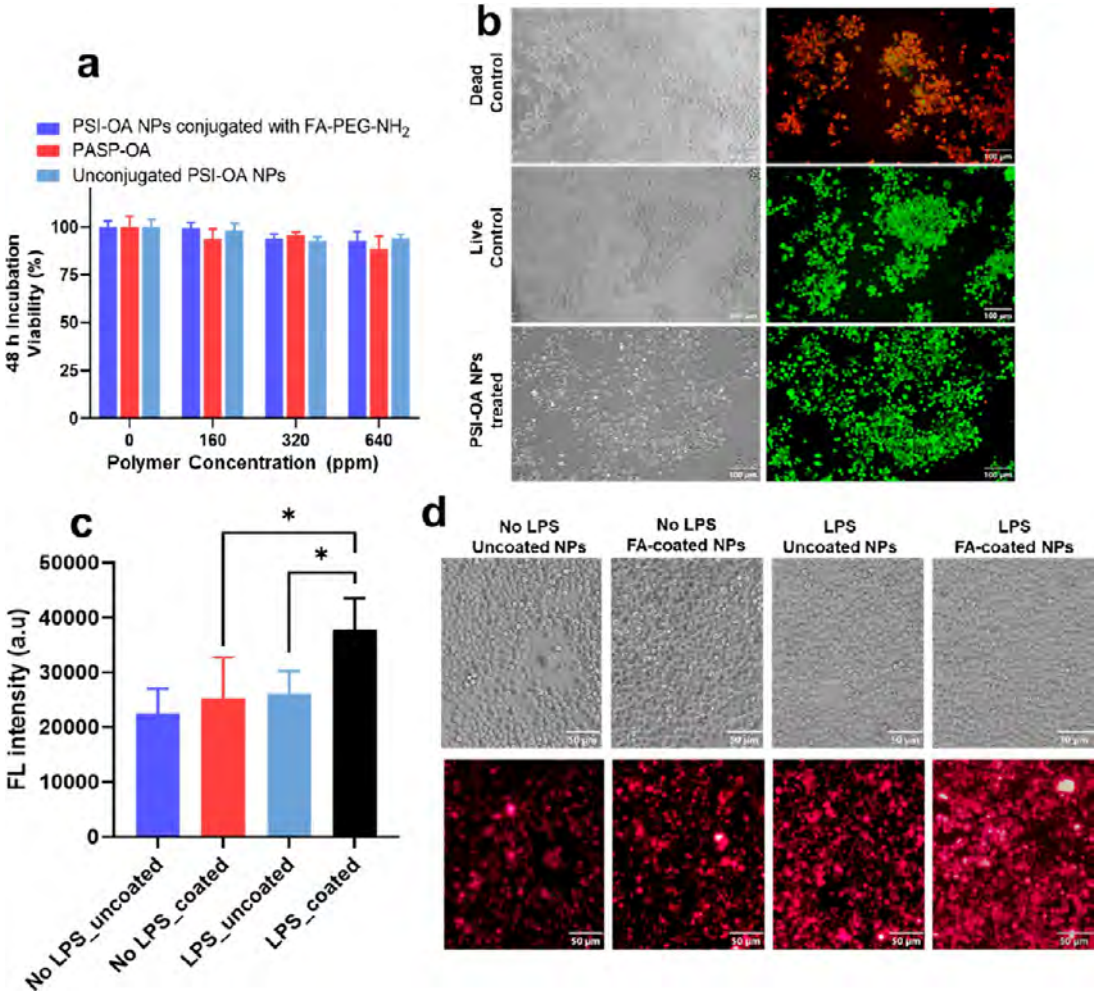

Figure 3. Viability and uptake study of RAW cells. (a) Viability of RAW cells in the presence of conjugated and unconjugated PSI-OA NPs as well as PASP-OA. The results are the average of 3 values for PrestoBlue assay, and no significant difference was found at the tested concentrations. The comparison of the statistical differences was carried out with respect to the cell control (0 μg/mL). (b) The microscopic images show live/dead cell assay in which green and red, respectively, represent live and dead cells. The left and right images are the brightfield and fluorescence images, respectively. The absence of red color further verifies the biocompatibility of the NPs. The scale bar is 100 μm (c) FL intensity of the cell lysate and (d) microscopic images of the cells for different treatment group. PSI-OA NPs were coated with FA-PEG for targeting purpose. The cells were treated either with LPS for stimulation or with the culture medium for 8 h followed by 2 h of NPs incubation. The scale bar is 50 μm. All the data are presented as the average of at least 5 replicates. * $P < 0.05$.

have been found to be nontoxic to different cells lines even at high concentration.[38] The biocompatibility of PASP- and PSI-based materials has been attributed to the peptide linkage bond in the backbone, similar to that of proteins.[16,38,39] The dead/live assay also confirmed the nontoxicity of the polymers of both cell lines.

The binding assay experiment was also carried out to assess the effect of FA-PEG surface conjugation on the NP uptake to the cells (Figure 3c,d). The comparison of the unstimulated and LPS-simulated RAW cells treated with FA-PEG-coated NPs revealed that the activated macrophage up-took a larger amount of FA-PEG-coated-NP. This demonstrated that the RAW cells under stimulated conditions were activated and could uptake more NPs. This was attributed to increased phagocytosis activity, enhanced surface receptor expression, secretion of different chemoattractants such as cytokines and chemokines, and altered signaling pathways such as the phosphoinositide 3-kinase (PI3K) pathway and mitogen-activated protein kinase (MAPK) pathway. These signaling pathways can promote the formation of membrane protrusions, facilitating efficient nanoparticle engulfment.[40]

Moreover, the comparison of uncoated and FA-PEG-coated NPs incubated with LPS-stimulated RAW cells (activated macrophage) showed that the cells up-took more FA-PEG-coated NPs. Furthermore, the microscopic images qualitatively supported the FL intensity results obtained by a microplate reader (Figure 3d). The presence of PEG-FA on the NPs enhanced their cellular uptake. While the present experiment does not elucidate the specific role of the PEG moiety, the enhanced uptake of nanoparticles (NPs) by activated macrophages can potentially be attributed to the expression of FA-receptors on the surface of inflamed cells.[41,42] It is worth noting that FA conjugation has been widely employed in drug delivery systems and nanocarriers containing bioactive therapeutics to facilitate cellular uptake by cancer cells and active macrophages.[43,44] The latter, when in an activated state, play a crucial role in various diseases, including rheumatoid arthritis, atherosclerosis, and vascular calcification.[43,44]

https://doi.org/10.1021/acsnano.3c03041
ACS Nano 2023, 17, 18775−18791

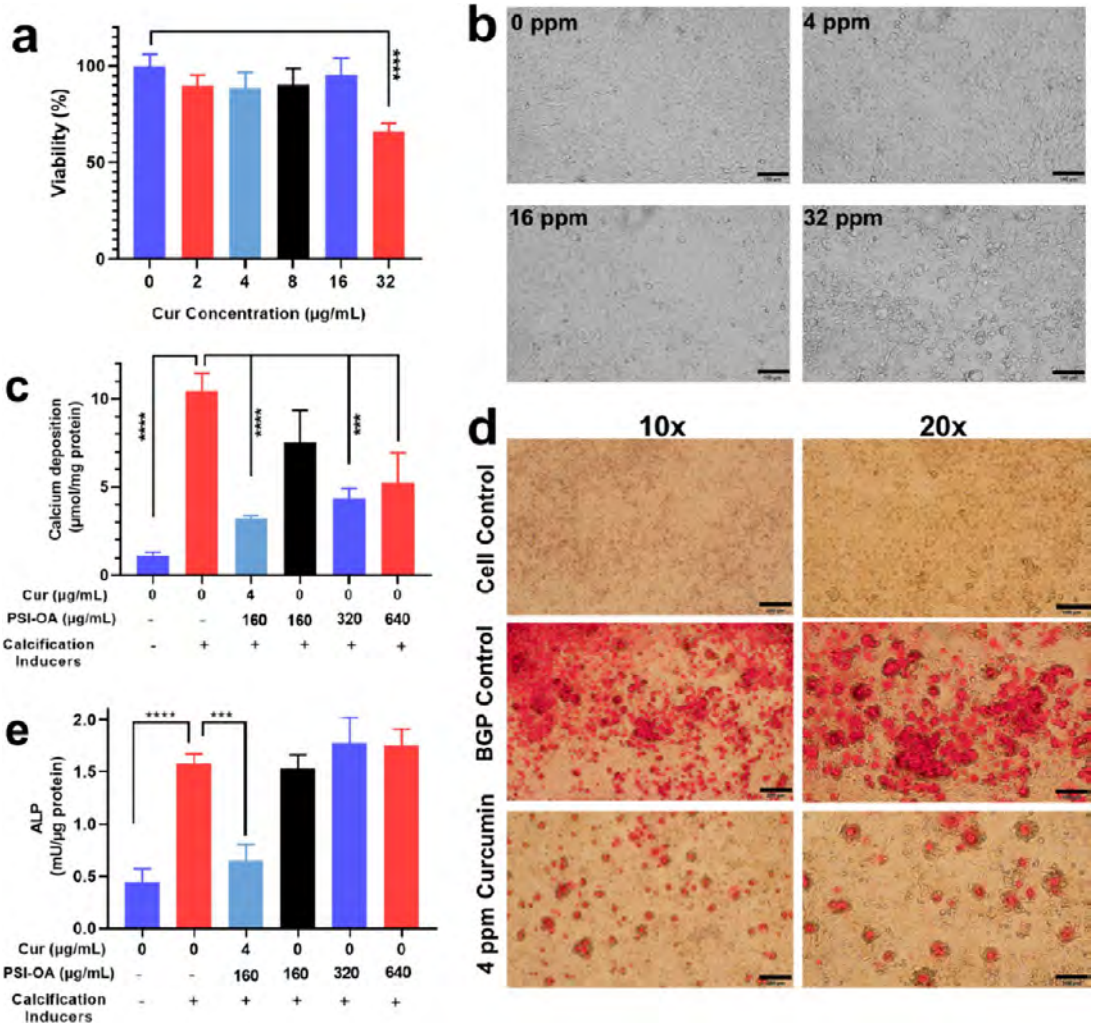

Figure 4. Viability and *in vitro* calcification of MOVAS treated with FA-PEG coated PSI-OA NPs and FA-PEG coated Cur-PSI-OA NPs. (a) Viability percentage of MOVAS incubated for 3 days at different NPs concentration, measured by PrestoBlue assay. (b) The optical microscopic images of the corresponding treatments show cell death with bubbling morphology at high Cur concentration. (c) The amount of deposited calcium normalized to protein content after 12 days of incubation with calcification inducers (containing βGP and $CaCl_2$), treated with PSI-OA NPs (160 μg/mL) and Cur-PSI-OA NPs (different concentrations). The cell medium was refreshed every 3 days. (d) MOVAS stained by Alizarin red to detect calcium deposition. Red indicates the presence of calcium deposits. "Cell control" is cells without any treatment, whereas "βGP control" is cells treated with calcification inducers in the absence of the NPs. "4 ppm of Curcumin" is the Cur-PSI-OA NPs containing 4 μg/mL Cur and 160 μg/mL PSI-OA. Scale bars in the left and right are 200 and 100 μm, respectively. (e) ALP activity of MOVAS with the same treatment indicates that (i) ALP was upregulated by the calcification inducers, (ii) Cur-PSI-OA reduced to approximately the basal level, and (iii) PSI NPs did not affect ALP activity. In all graphs, data are presented as mean ± SD of at least 3 replicates. * $P < 0.05$, ** $P < 0.01$, *** $P < 0.001$, **** $P < 0.0001$.

Viability and *In Vitro* Calcification of MOVAS. As shown in Figure 3a,b and Figure S4, the neat NPs did not have toxicity at the tested concentrations to the cells. Herein, the effect of varying concentrations of Cur was tested on the cell viability of MOVAS (Figure 4a). After 3 days of incubation of MOVAS with the NPs, no significant toxicity was noticed except for 32 μg/mL of Cur. As seen in the microscopic images of 32 μg/mL Cur (equivalent to 1280 μg/mL NPs), there is cell bubbling and viability is reduced to around 55% with respect to the cell control (Figure 4b). Although highly active and useful for different pathological conditions, Cur could become highly toxic even to the normal cells at high concentrations. Such a toxicity level has been reported in several studies as well.[45,46]

Vascular smooth muscle cells are known as the main mediator for this disease through trans-differentiation to osteogenic cells. Thus, *in vitro* calcification of MOVAS is evaluated herein. MOVAS is an established cell line for studying *in vitro* calcification.[47−49] Culture of MOVAS for 12 days in calcification media (DMEM supplemented with 10 mM βGP and 1 mM $CaCl_2$, 50 μg/mL of L-ascorbic acid) led to extensive mineralization. Such a culture condition was found to increase the level of calcium deposition by around 8 times (Figure 4c,d). This is attributed to trans-differentiation of MOVAS to osteogenic cells, thereby upregulating bone gene markers (e.g., ALP) (Figure 4e). ALP is a well-known enzyme that catalyzes the hydrolysis of pyrophosphates to inorganic phosphate. While the former is regarded as a potent inhibitor, the latter serves as an inducer for calcium deposition.[47,48]

For the treatment, as discussed above, the cells were viable when treated with the PSI-OA NPs up to the tested concentration of 640 μg/mL (3 days of incubation). However,

https://doi.org/10.1021/acsnano.3c03041
ACS Nano 2023, 17, 18775−18791

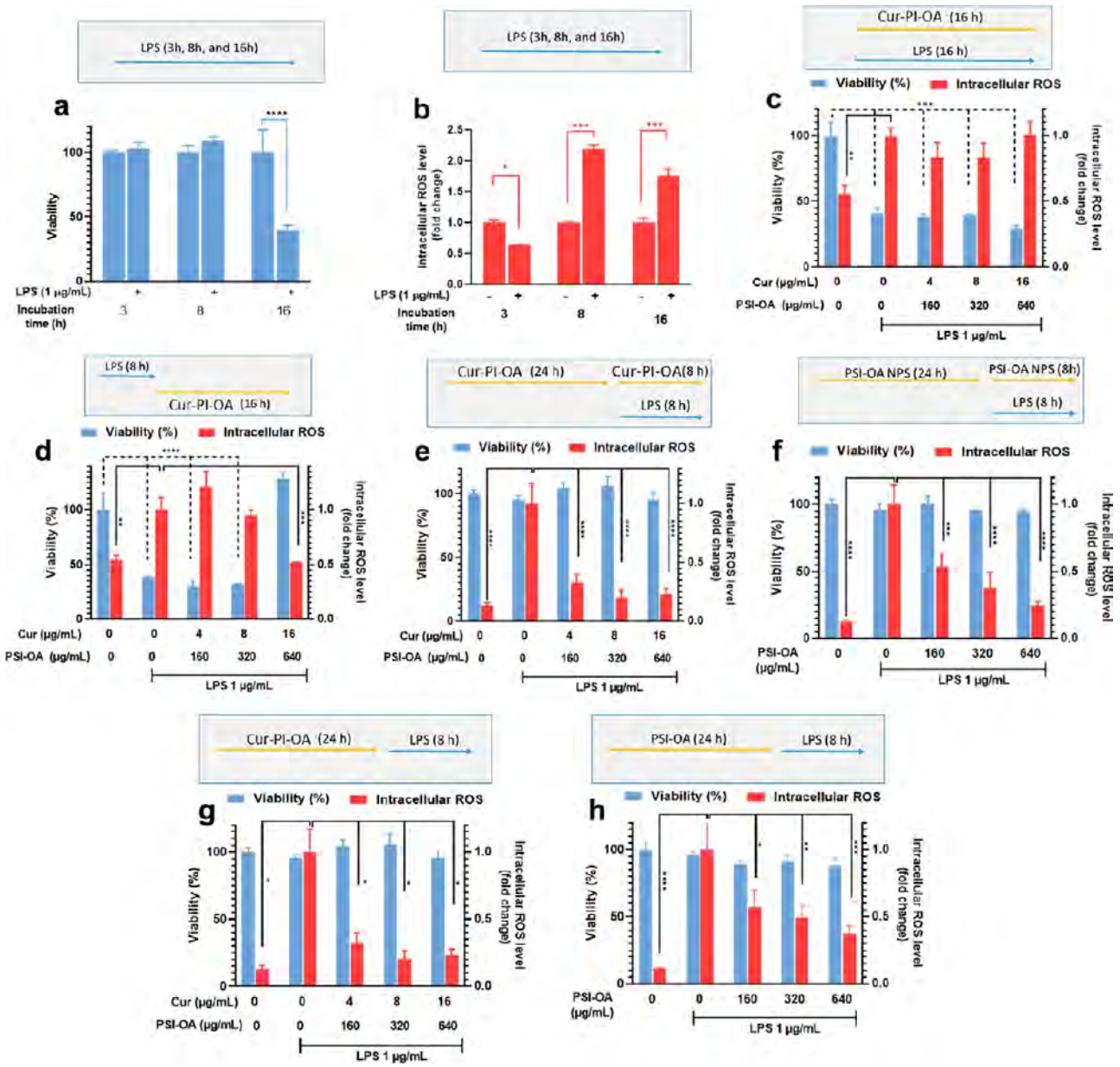

Figure 5. Effect of FA-PEG-coated NPs on viability and intracellular ROS level of RAW cells. (a and b) Optimization of LPS incubation duration, in the absence of the NPs: (a) viability and (b) ROS. (c–h) Treatment of RAW cells with (c) simultaneously Cur-PSI-OA NPs and LPS for 16 h; (d) LPS stimulation for 8 h followed by Cur-PSI-OA NPs for 16 h; (e) Cur-PSI-OA NPs for 24 h followed by simultaneous Cur-PSI-OA NPs and LPS for 8 h; (f) PSI-OA NPs for 24 h, followed by simultaneous LPS and PSI-OA NPs for 8 h; (g) Cur-PSI-OA NPs for 24 h followed by LPS for 8 h; (h) PSI-OA NPs for 24 h followed by LPS for 8 h. LPS concentration in all experiments was 1 μg/mL. All the data are presented as the average of at least 3 replicates. * $P < 0.05$, ** $P < 0.01$, *** $P < 0.001$, **** $P < 0.0001$.

as indicated above, Cur at high concentration (32 μg/mL) was toxic to the cells after 3 days of incubation. Such a long incubation duration was chosen because the media should be changed every 3 days for 2 weeks to induce MOVAS calcification. Therefore, the concentration range for pure PSI-OA NPs and Curcumin in Cur-PSI-OA NPs were chosen to be up to 640 and 4 μg/mL, respectively. It should also be added that Cur at 8 and 16 μg/mL was toxic to MOVAS for 2 weeks of incubation, and no viable cell was detected at the end of the experiment. Cur-PSI-OA NPs (4 μg/mL Cur), however, were highly efficient in preventing osteogenic differentiation as the level of ALP was not elevated. As a consequence of such prevention, calcium deposition was also inhibited significantly. PSI-OA NPs did not have a significant impact on ALP activity. These results are in good agreement with our previous results on the effects of PASP and PSI NPs on the MOVAS calcification, where the polymers prevented calcification but not osteogenic differentiation.

Anti-ROS Behavior of the PSI-OA NPs (with and without Cur). Our previous study revealed that PASP has an anti-ROS effect both in macrophages (J774) treated with LPS and in MOVAS treated with iron. The iron chelation ability of PASP was investigated, showing that PASP suppresses the Fenton reaction, which is responsible for generation of hydroxyl radicals. Accordingly, the low ROS level in these cell lines was attributed to iron chelation of PASP. In this study, we also tested the anti-ROS effects of the prepared PSI-OA NPs (with and without Cur) on RAW cells stimulated by

https://doi.org/10.1021/acsnano.3c03041
ACS Nano 2023, 17, 18775–18791

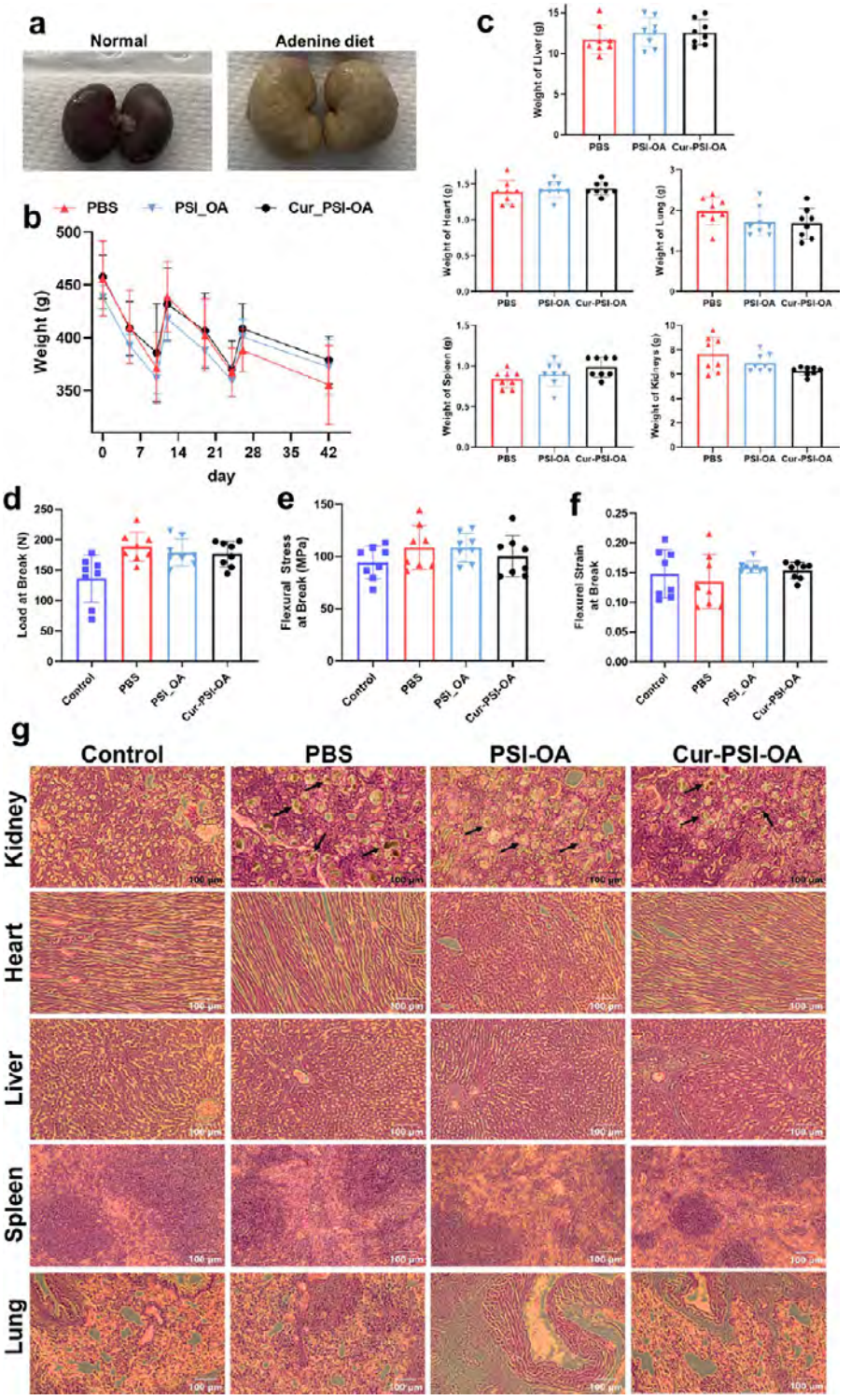

Figure 6. Weight change of animals and their organs as well as evaluation of side-effects of the treatments. Experiments were performed with FA-PEG-coated NPs. (a) Digital photographs of the collected normal and injured kidneys from animals with normal chow and adenine diets. (b) Animals' weight over 4 weeks of adenine diet followed by 2 weeks of CaP diet. To compensate weight loss larger than 15%, the diet was changed to normal chow diet for 1−2 days. (c) The weight of different organs of the rats from different treatment groups. (d−f) Mechanical properties of the harvested bones in terms of (a) load at break, (b) flexural stress, and (c) flexural strain at break for different groups of animals. No significant difference in any of these values was found, indicating that the treatment does not adversely affect the bone integrity. (g) Histological analysis of organs in different treatment groups of PBS and PASP compared with the control group. Scale bar is 100 μm. Black arrows in the histological images of the kidney show the crystallized 2,8-dihydroxyadenine in the kidney, resulting in renal failure.

LPS (Figure 5). In the first experiment, LPS incubation time was optimized, in the absence of any polymer treatment, and it was found that 16 h of LPS incubation caused toxicity although ROS was elevated (Figure 5b). The optimum duration for LPS treatment was found to be 8 h, where cell viability was not adversely affected, while ROS level was high.

https://doi.org/10.1021/acsnano.3c03041
ACS Nano 2023, 17, 18775−18791

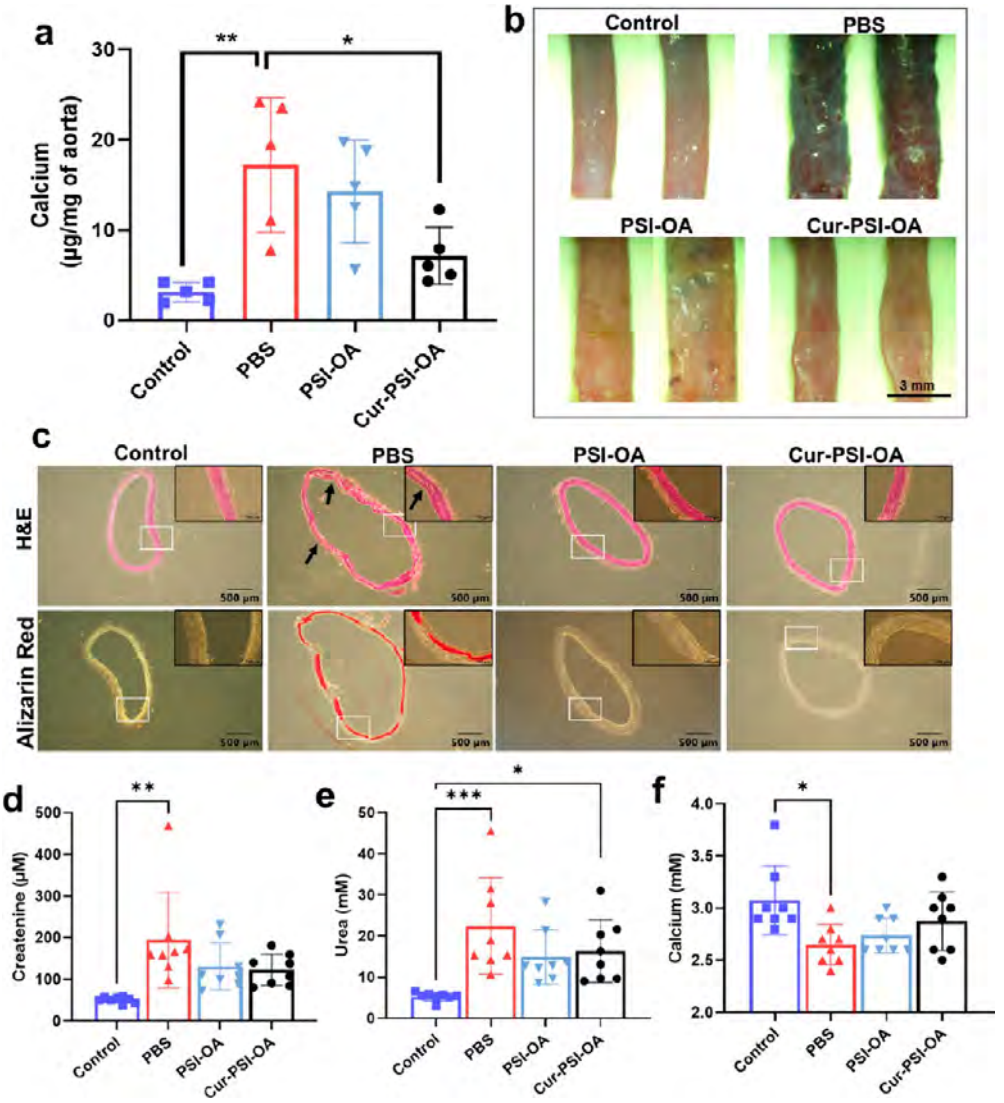

Figure 7. Inhibition of vascular calcification by Cur-PSI-OA NPs. Experiments were performed with FA-PEG-coated NPs. (a) Quantitative measurement of calcium normalized to the dry weight of aortas. (b) Microscopic images of the aortas stained with alizarin red S. Calcium deposition is visible in dark red. The scale bar is 3 mm. (c) Histological analysis of the aortas harvested from animals in different treatment groups. The sections were stained with H&E and alizarin red to detect morphological changes and calcium deposition, respectively. The white rectangles are the areas that were magnified in the insets. The black arrows show damage to the aorta. The scale bars of the main and the inset images are 500 and 100 μm.

To evaluate if the above-mentioned toxicity could be alleviated by the polymer, RAW cells were treated with LPS (1 μg/mL) and Cur-PSI-OA NPs simultaneously for 16 h (Figure 5c). It was found that neither was toxicity alleviated nor ROS level attenuated even at high Cur concentration (16 μg/mL). In the next experiment, after 8 h of LPS stimulation, the cells were treated with Cur-PSI-OA NPs for 16 h (Figure 5d). Even though the media for the polymer treatment lacked LPS, the cell viability was severely affected, suggesting that after LPS removal, the consequences of its action remained effective, generating a high ROS level and posing toxicity. Nevertheless, when the Cur concentration was 16 μg/mL, the cell viability and ROS level were close to those of the cell control (Figure 5d), indicating the protective role of this phenolic natural compound.

In the next set of experiments, after the cell pretreatment with the NPs (with and without Cur), simultaneous LPS and NP treatment was carried out for 8 h (see the order and time frame in Figure 5e,f). The presence of either Cur or PSI-OA NPs significantly lowered the ROS level without a noticeable change in the viability.

In the final set of anti-ROS experiments (Figure 5g,h), pretreatment of the cell with Cur-PSI-OA NPs and pure NPs followed by 8 h of LPS stimulation showed a similar trend as Figure 5e,f. These results further verify the independent anti-ROS activity of both polymer and Cur. Overall, these results demonstrate the anti-ROS activity of both Cur and PSI-OA NPs. Cur is a well-known natural small molecule polyphenolic compound with a variety of health-promoting properties, such as anti-inflammatory and antioxidant activities. Cur inhibits the oxidation of proteins and DNA. At the enzymatic level, Cur inhibits lipoxygenase/cyclooxygenase and xanthine dehydrogenase/oxidase, which are two pro-ROS enzymes, while upregulating superoxide dismutase and glutathione peroxidase, the two notable anti-ROS enzymes. Regarding the polymer, however, it is believed that the anti-ROS mainly originates

https://doi.org/10.1021/acsnano.3c03041
ACS Nano 2023, 17, 18775−18791

from the iron chelation activity of the polymer, as discussed in our previous work.

Vascular Anticalcification of the NPs in CKD Rat Model. In this study, renal failure was induced by using an adenine diet for 4 weeks,[50] followed by a 2 week calcium and phosphate diet to induce vascular calcification.[51] At low concentration, adenine is metabolized by xanthine oxidase and is converted into uric acid, thereby increasing uric acid and blood urea nitrogen level which are known as important risk factors for atherosclerosis.[52,53] At high concentrations, adenine is oxidized to highly insoluble 2,8-dihydroxyadenine by xanthine dehydrogenase (XDH). 2,8-Dihydroxyadenine is then crystallized and accumulated in the kidneys with minimal excretion, leading to renal failure. As a result, depending on the severity of failure, a mineral imbalance is induced, eventuating in their deposition in soft tissues, including vasculature.[51,54] Compared to other models of renal failure, this model requires no surgery and has no mortality rate, although it has a weight loss disadvantage.[54−57] Figure 6a presents photographs of healthy and injured kidneys harvested from animals in the healthy control and PBS injected disease group, respectively. Figure 6b,c indicates the weight of animals and their respective organs in different groups. As seen, the animals with the adenine diet exhibited a fast weight loss due to both its nephrotoxicity and its amino-acid deficiency (2.5% protein). To compensate the weight loss, when it was close to or greater than 15%, the animals were given a normal chow diet for 1−2 days. Although the CaP diet contained normal protein content, the animals in both groups still showed weight loss which could be due to renal failure and vascular calcification. The average weights of the animals and their respective organs in different groups were not significantly different (Figure 6b,c).

Loss of bone integrity is the most common side effect in chelation therapy for the treatment of vascular calcification. For instance, a recent clinical study with sodium thiosulfate (a strong calcium chelator) showed that bone mineral density of the total hip decreased, despite its positive preventive impact on the progression of calcification.[58] The high calcium-binding ability of aspartic acid has also been employed for targeting of drug-loaded NPs to bone.[59−62] As the hydrolysis product of PSI-OA, which is PASP-OA, could have strong chelation ability, to evaluate their possible side effect, the mechanical integrity of femoral bones of the rats was measured (Figure 6d−f). The average load at break for Control, PBS-, PSI-OA NPs, and Cur-PSI-OA-treated groups were 136.3, 188.2, 178.9, and 176.6 N, while their flexural stress values were 94.3, 108.6, 108.6, and 100.2 MPa, respectively. Although the average values show a slight variation in different groups, the differences were not found to be statistically significant. Moreover, histological analysis (Figure 6g) indicated that the treatment caused no significant change in heart, liver, and spleen organs. It should be noted however that the lung samples in all groups including the control showed a significant collapse in the alveoli structure, which is due to the carbon dioxide euthanasia method used in this study. Such severe histological changes in lungs are in agreement with other studies as well.[63,64] The histological images of the kidney also showed severe damage to the structure of tubules induced by the crystallization of 2,8-dihydroxyadenine, which are marked by black arrows (Figure 6g). The latter is formed through oxidation of adenine by xanthine dehydrogenase and is water insoluble, which is thus deposited in the kidney and bladder with negligible clearance.[65]

Two animals in the PBS group on the last week of the experiment developed signs of leg paralysis. Their aortas showed increased blood vessel diameters when compared with normal aortas. Staining of the aorta with alizarin red confirmed significant calcification (Figure 7a). While calcium deposition along the aorta was not uniform and consistent, it was found that calcification was more noticeable in the abdominal aorta, rather than the thoracic part. Furthermore, calcification between different animals in the same group could vary significantly. Quantitative measurement of aortic calcium also indicated that the PBS-treated group as compared to the normal (healthy) group developed severe calcium. Treatment with PSI-OA NPs did not significantly reduce the calcium level at the dose tested. Increasing the dose might provide a better outcome. The calcium level in the Cur-PSI-OA group was significantly lower than that in the PBS group (Figure 7b). This indicates the efficacy of the treatment in the prevention of calcification, which could originate from anti-inflammatory activity of Cur. These *in vivo* results are in agreement with *in vitro* calcification of MOVAS presented above.

Histological analyses of one aorta from each group were also carried out respectively by H&E and alizarin red staining of the sections to investigate the morphological changes and calcium deposition (Figure 7c). Severe damage to the structure of aorta was seen in the PBS group (black arrows) as compared to other aortas. As the results demonstrated, an extensive calcium deposition could be seen in the PBS-treated group. The results were also supported by those of H&E staining where the aorta was notably damaged.

The results of serum analysis are shown in Figure 7d−f. The mean creatinine concentration of the serum of healthy rats was about 60 μM, whereas in adenine-fed rats this increased to about 170 μM (Figure 7d). Serum urea showed a similar trend, with a 4-times greater level of urea in the adenine-fed rats than in the healthy rats (Figure 7e). The increase in creatinine and urea is common in nearly all CKD animal models and is indicative of kidney dysfunction. As seen, neither PSI-OA nor Cur-PSI-OA contributed to statistically meaningful lower creatinine levels. As for the urea, these treatments were not effective enough in serum urea reduction, thereby suggesting that both PSI-OA and Cur-PSI-OA are not able to prevent kidney damage induced by adenine and 2,8-precipitation of dihydroxyadenine. The calcium concentration of the serum in the healthy rats was higher than that of PBS-treated rats which could be attributed to its calcium complexation with phosphate and subsequent precipitation in different organs (Figure 7f). Nevertheless, the serum calcium levels in PSI-OA and Cur-PSI-OA were increased when compared to that in the PBA group (no statistically significant difference was found, although calcium is supplemented in the diet). These results indicate that PSI-OA and Cur-PSI-OA, upon hydrolysis and conversion to PASP, could form a stable complex with free calcium and inhibit their precipitation. The average serum levels of AST and ALT were nearly similar in all treatment groups, suggesting that the liver function is not influenced either positively or negatively by the diet and the treatments, further verifying the results of histological analysis shown above (Figure S5). It is worthwhile to mention that adenine diet has found to be nontoxic to the liver.[66] This also demonstrates the fact that frequent PSI-OA and Cur-PSI-OA injections at relatively high concentration do not lead to liver toxicity, confirming the cell biocompatibility results shown above.

https://doi.org/10.1021/acsnano.3c03041
ACS Nano 2023, 17, 18775−18791

CONCLUSIONS

This paper presents PSI-OA NPs as an effective anticalcification agent and as a promising carrier for the loading, release, and delivery of hydrophobic drugs. The NPs were prepared by emulsion evaporation and were shown to have the ability to be easily conjugated with a variety of amine-containing molecules. Interestingly, the NPs were stable at slightly acidic conditions (pH < 5.5) for a long time, while under simulated physiological conditions, they were disintegrated and solubilized into hydrophilic PASP derivatives. Such a conversion was highly useful as the payload was realized to be released in accordance with the dissolution profile such that complete release occurred after 48 h at physiological condition. Under acidic conditions, however, the cumulative release reached only 30% after 1 week. The prepared NPs had anti-ROS activity on the LPS-stimulated RAW cells. Incorporation of Cur into the NPs further improved the anti-ROS activity. Furthermore, the Cur-PSI-OA NPs prevented osteogenic differentiation of MOVAS, thereby inhibiting its calcification under a calcifying medium. The polymer NPs without Cur, though they reduced calcium deposition, were not efficacious in the inhibition of trans-differentiation. The Cur-PSI-OA NPs were also highly effective in treating *in vivo* vascular calcification of uremic rat models. The calcium level in the aorta was significantly reduced without adversely affecting the bone integrity and/or imposing toxicity/damage to other organs. Considering their attractive features such as biocompatibility, chelation activity, sustained drug release as well as reactivity for simple conjugation, the developed NPs are expected to gain a great deal of attention for biomedical applications in general and for the treatment of cardiovascular diseases in particular.

MATERIALS AND METHODS

Synthesis of Poly(succinimide). Poly(succinimide) (PSI) was synthesized through conventional poly condensation reactions of aspartic acid, as established previously.[67,68] Briefly, aspartic acid (Sigma,14 gr, Mw = 133.11 g/mol, 105.17 mmol), H_3PO_4 (85 wt % in H_2O, Sigma, 1 mL), and sulfolane (Sigma, 56 mL) were poured into a 100 mL flask placed in an oil bath at 180 °C under nitrogen gas flow with mechanical stirring (150 rpm). After 5 h, the solution was precipitated in a large amount of deionized (DI) water. The PSI polymer powder was washed several times with DI water to remove excess catalyst and solvent and finally dried in a freeze drier. Chemical structures of the synthesized polymers were evaluated by a Fourier-transform infrared spectroscopy (FTIR) instrument (Nicolet 5700 FT-IR) equipped with an attenuated total reflectance accessory (ATR) and the diamond internal reflection element. The spectra are the average of 16 scans captured in the wavenumber range of 4000−400 cm^{-1}. A proton nuclear magnetic resonance (^1H NMR) (Bruker Ascend 400 MHz NMR) spectrometer operating at 400.13 MHz and 25 °C was also utilized for characterization of PSI in d6-DMSO as the solvent, and the chemical shifts are reported in ppm (δ). The molecular weight of the prepared PASP was determined using an aqueous gel permeation chromatography (GPC) Agilent GPC/SEC with a dual angle laser light scattering detector, viscometer, and differential refractive index detector calibrated by ethylene oxide standard.

Synthesis of Oleylamine-Modified Poly(succinimide). Regarding the modification with oleylamine (OA), in a typical reaction, 10 mL of 10% w/v PSI in DMF was mixed with 995 μL of OA and incubated under a nitrogen atmosphere at 70 °C for 12 h. This feed concentration of OA (Mw = 267.5 g/mol) is 30 mol % with respect to succinimide units (Mw of repeat unit = 98 g/mol), and thus considering the yield of 100%, 30% of the polymer is modified/grafted with OA. After 12 h, the mixture was cooled, the polymer was washed with methanol to remove unreacted OA as well as excess DMF, and finally the polymer was freeze-dried.

Synthesis of PSI-OA NPs by Emulsion Evaporation Method. Oleylamine-modified poly(succinimide) (PSI-OA) (20 mg) was dissolved in DCM (1 mL) overnight in a tightly sealed Eppendorf tube. For the water phase, 10 mL of PVA solution in DI water was used. In the case of partially and fully hydrolyzed PVA, the concentrations of 2.5 and 1 wt % were used, respectively. The polymer solution in DCM (1 mL, 20 mg/mL) was added to 10 mL of PVA solution in a 20 mL glass vial, and the mixture was homogenized for 2 min at 7000 rpm. For partially hydrolyzed PVA, the lowest homogenization speed of 1000 rpm was used in order to prevent foaming in the emulsions. Next, the emulsions were placed in a water bath at room temperature and sonicated for 2 min (Amplitude 50%, Pulse: 2 s on and 2 s off). The inclusion of a water bath during the sonication process is crucial to maintain control over the emulsion temperature. Without a water bath, the sonication process has the potential to cause rapid boiling of DCM (boiling point of 40 °C), leading to destabilization of the emulsions. After the sonication, the emulsion was placed in a water bath at 37 °C for slow evaporation of DCM (and thus polymer solidification) with the highest stirring speed (1600 rpm) with magnetic bar of 1 cm. For partially hydrolyzed PVA, room-temperature drying was adopted, as increasing the temperature to even 35 °C destabilized the emulsion through foaming. After 4 h, the emulsions were completely turned into solidified polymeric NPs. The NPs were washed twice with DI water to remove PVA, and the NPs were redispersed in water by pipetting. Dynamic light scattering (DLS) (Zetasizer Nano ZS) was employed to determine the size and zeta potential of the NPs. After the NPs were washed, to measure the size, they were diluted in DI water (final concentration of 0.2 mg/mL) and mixed well, and measurement was carried out without filtering. Transmission electron microscopy (TEM) images were taken on a JEOL-JEM-1010 TEM, operating at an accelerating voltage of 80 kV.

Dissolution Study of PSI NPs under Different Conditions. In a typical dissolution experiment, PSI-OA polymer dispersion (2 mg/mL, 20 μL) was added to the following solutions/buffers (180 μL) with different pH values. Acetate buffer with pH 4.5 (50 mM, sodium acetate/acetic acid); PBS with pH 7.4 at different strengths of 1×, 2.5×, 5×, and 10× and potassium phosphate buffer with pH 8; human plasma; FBS; and DI water were used for the dissolution study. The final concentration of the polymer in the solution is 200 μg/mL. The mixture was transferred to a 96-well plate. It is important to highlight that when low concentrations of NPs are used in the dissolution experiment, they do not generate significant turbidity. Consequently, the complete dissolution of NPs does not lead to substantial or meaningful decreases in the optical density (OD) values; 200 μg/mL was found to be an optimum concentration in this regard. The plate was placed in a microplate reader operating at 37 °C (SpectroStar Nano, Model BMG LabTech), and the OD values at 350 nm over time were obtained.

Differential Scanning Calorimetry (DSC)/Thermogravimetric Analysis (TGA). 5−10 mg of the vacuum-dried NPs or Cur powder was weighed in a crucible and placed into the DSC instrument (Mettler Toledo, TGA/DSC, USA). The DSC and TGA runs were conducted with a temperature range of 50−500 °C and a heating rate of 20 °C/min.

Conjugation of Cy5-NH_2 and Folic-PEG-NH_2 to PSI-OA NPs. To the PSI NPs dispersed in DI water was added Cy5-NH_2 at different concentrations (final concentrations of up to 16 μM). The final concentration of the PSI NPs is 0.5 mg/mL. The mixtures were incubated at room temperature for 4 h followed by washing to remove the unreacted Cy5-NH_2. The fluorescence intensity of the supernatant was measured to evaluate the amount of the Cy5-NH_2 conjugation. Regarding the conjugation of FA-PEG-NH_2, different mass ratios of FA-PEG-NH_2 to PSI NPs (0.5:10, 1:10, 2:10, and 5:10) were tested. FA-PEG-NH_2 was purchased from RuixiBiotech Co. Ltd. The molecular weight of the PEG unit is 5000 g/mol. One end of the PEG is capped with folate, while the other is NH_2. The final concentration of the PSI NPs in the reactions is 1 mg/mL. The

https://doi.org/10.1021/acsnano.3c03041
ACS Nano 2023, 17, 18775−18791

reactions were carried out for 4 h at room temperature in DI water without the use of any catalysts followed by twice washing with DI water (separation with centrifugation at 16000 *g* for 15 min, redispersion with pipetting). After washing, the zeta potential and the size of the NPs were measured. ATR-FTIR was also used to analyze the changes in the surface groups of the PSI-OA NPs.

Encapsulation of Cur into PSI-OA NPs. For Cur loading, the emulsion evaporation method was used as described above, except for the inclusion of Cur into the polymer solution in DCM. Briefly, PSI-OA (20 mg) and Cur (500 μg) were dissolved in DCM (1 mL). To ensure complete dissolution of Cur, 2 μL of DMSO was added to the DCM solution. The solution was emulsified in the water phase, containing 2.5% partially hydrolyzed PVA and incubated for 5 h at room temperature to evaporate DCM. The encapsulation efficiency (EE%) was calculated using the following formulas, where W_t is the final amount of Cur in the dispersion and W_i is the total Cur amount initially added for the NP preparation. W_t was measured by destructing the NPs in DMSO and measuring the absorbance at 424 nm.

$$\text{encapsulation efficiency (EE\%)} = (W_t/W_i) \times 100\% \quad (1)$$

Release of Cur-PSI-OA NPs. 2 mg/mL of Cur-PSI-OA NPs was dispersed in different release media (acetate buffer pH 4.5, PBS pH 7.4, and potassium phosphate buffer pH 8), containing 0.2 wt % tween 80 and incubated on a shaker at 37 °C for 96 h. At different time points, 250 μL of the dispersion was taken and centrifuged at 25000*g* for 15 min. The supernatant was taken, and its absorbance was read at 424 nm using a SpectroStar Nano, Model BMG LabTech. For pH 7.4 and 8, to calculate the release percentage, the absorbance at each time point was divided by that at 48 h (complete disintegration of the carrier, equivalent to 100% release). However, for pH 4.5, as the complete (100%) release did not occur even after 96 h, the NPs were destructed (at time = t_0) with DMSO and the absorbance of the total amount of Cur was measured. The absorbance at each point was then divided by the time at t_0 to calculate the release percentage.

Cell Culture. Aortic smooth muscle cells (MOVAS, CRL-2797), and macrophage RAW264.7 cells were purchased from the American Type Culture Collection (ATCC). The culture medium for both cell lines was DMEM (Sigma D6046, 1000 mg/L glucose) supplemented with FBS (10%), and penicillin−streptomycin (100 U each/mL). The cells were cultured at 37 °C with 5% CO_2.

Cytotoxicity Study. The cells (MOVAS or RAW264.7) were seeded into 96-well plates at a density of 10,000 cells/well. After 24 h, the media of the cells were aspirated and incubated with different concentrations of the NPs. The cell viability was determined with PrestoBlue reagent (ex/em = 560/590 nm). The cells were washed and incubated with PrestoBlue (diluted 10 times in Dulbecco's phosphate-buffered saline (dPBS) according to manufacturer instructions) for 30 min at 37 °C. The fluorescence of the control group (without treatment) was considered as 100% cell viability. Dead control group was treated with water/methanol solution (7/3 vol/vol) for 30 min. A live/dead cell imaging kit (Thermofisher, L3224) was used according to the supplier protocol. Briefly, Calcein AM (5 μL, 4 mM) and ethidium homodimer-1 (EthD-1) (20 μL, 2 mM) were added to 10 mL of DPBS and mixed well to create the staining solution. The former and the latter, respectively, stain the live and dead cells green and red. After the cell medium was removed, the staining solution (100 μL) was added to each well and incubated for 30 min at room temperature. The fluorescence images of the cells were taken with an inverted fluorescence microscope (CKX53, Olympus) using a TRITC filter.

Uptake Studies on RAW Cells. For the uptake study, RAW cells with a density of 10,000 per well were seeded in 96 well-plates using the culture medium mentioned above. The cells were incubated overnight and then treated with LPS (1 μg/mL) for 8 h for stimulation/activation. After LPS stimulation, the cells were treated with Cy5-labeled PSI-OA NPs. Cy5 was conjugated to the backbone of the polymer before the formation of the NPs (discussed below). Cy5 conjugation in the uptake studies was carried out before particle formation to ensure that the dissolution of the NPs did not result in the loss of FL molecules for detection and measurement. The NPs (100 μg/mL) dispersed in the culture medium were incubated for 2 h with the cells. After 2 h, the medium was discarded and the cells were lysed with 1% tween in dPBS (100 μL). The fluorescence intensity (FL) of the cell lysate was measured by a BMG LabTech microplate reader Model BMG LabTech. The same procedure was conducted in another 96-well plates without lysing the cells for FL microscopic purpose. Regarding the conjugation of Cy5 to PSI-OA, Cy5-NH_2 (5 μL, 4 mM in DMSO) was added to PSI solution in DMF/DMSO (50/50 v/v) (500 μL, 50 mg/mL), and the mixture was gently stirred overnight at room temperature. The solvent mixture was used because PSI-OA was not well-soluble in DMSO and Cy5 stock was in DMSO. To make sure DMSO of Cy5 did not disturb the solubility of the polymer, we first dissolved the polymer in DMF/DMO 50/50 to make sure it was well soluble. The solution was then precipitated in 5 mL of methanol and washed twice to remove unreacted Cy5-NH_2. The polymer was then dried overnight in a vacuum oven at 50 °C.

***In Vitro* Calcification of MOVAS: Measurements of Calcium, ALP, and Protein.** For *in vitro* calcification, MOVAS was seeded into 96-well plates at a density of 5,000 cells/well. One day after seeding, the cells were treated with calcification inducers and polymer NPs. The calcification medium was the growth medium stated above supplemented with βGP 10 mM, $CaCl_2$ 1 mM, and ascorbic acid 50 μg/mL (cells treated with this medium only were referred to as the βGP control). Calcification medium containing the polymer NPs (up to 640 ppm) was added to the cells, and the medium was changed every 3 days. After 12 days of incubation, the medium was aspirated, followed by washing with dPBS. After 15 min of incubation at 37 °C with Tryple Express, the cells were detached and were used for further steps. To measure protein, 2 wt % Triton X-100 (without acid) was added, followed by incubation at 37 °C for 1 h. However, to measure calcium, 2% Triton X-100 in 1.2 M HCl was added to the wells (50 μL for 96-well plate) and the mixture was incubated at 37 °C for 1 h. Triton X-100 lyses the cells while HCl dissolves all calcium salts. Calcium concentrations were measured by a calcium colorimetric assay kit (Sigma, MAK022) by measuring the absorbance at 575 nm. Briefly, 25 μL of sample or standard solution was added to a 96-well plate. Then, 45 μL of the chromogenic reagent was added to the wells followed by the addition of 30 μL of the buffer assay reagent. The mixture was kept in the dark for 15 min at room temperature, and the absorbance was recorded at 575 nm. A linear standard curve was generated from 31.25 to 1000 μM of calcium, and accordingly, the calcium levels of the samples were calculated. Alkaline Phosphatase (ALP) Diethanolamine Activity Kit (Sigma AP0100) was used to measure the ALP level in the cell lysate. The assay uses p-nitrophenyl phosphate (pNPP) as substrate, which is converted to ionic phosphate and p-nitrophenol in the presence of ALP. p-Nitrophenol has a yellow color, and a linear standard curve in the range of 0.0625−0.5 unit/mL of ALP was achieved at 405 nm. 20 μL of the sample or standard ALP solutions, 160 μL of the buffer reagent, and 20 μL of freshly prepared p-nitrophenyl phosphate (pNPP) (67 mM in DI water) were mixed and incubated in the dark at room temperature for 30 min, and absorbance was recorded at 405 nm. The ALP level was normalized to the calculated protein level by BCA assay.

Alizarin Red Staining. After 12 days of incubation, the cells were washed with dPBS and fixed with a 4% paraformaldehyde solution in dPBS for 15 min at room temperature. Then, the cells were washed with dPBS twice, and a freshly prepared and filtered solution of alizarin red (100 μL, 1 wt % in DI water, pH 4.1) was added to the wells. The cells were incubated for 10 min at room temperature, and the staining solution was aspirated. The cells were washed twice with dPBS and observed with an inverted optical microscope (CKX53, Olympus).

Intracellular ROS Studies. RAW264.7 cells (seeding density of 10,000/well in 96-well plate) were treated with different concentrations of polymer NPs and Cur. The treatment time frame is presented above its respective graph in the Results and Discussion. The intracellular ROS level was assessed using a dichlorofluorescein diacetate (DCFDA) assay as previously described.[69−72] Briefly, the

https://doi.org/10.1021/acsnano.3c03041
ACS Nano 2023, 17, 18775−18791

cells were washed once with dPBS and incubated with DCFDA solution in dPBS (100 μL, 25 μM) for 30 min followed by direct measurement of fluorescence intensity (Ex/Em = 485/535 nm) using a FLUOstar Omega BMG Plate Reader. The fluorescence value of the medium (without cells) was subtracted from that of each experimental group. ROS levels were calculated using eq 1:

$$\text{ROS level (fold change)} = \frac{F_{\text{treatment}}}{F_{\text{control}}} \quad (2)$$

where $F_{\text{treatment}}$ is the fluorescence intensity of the treated cells, while the F_{control} value is that of cells without any additional stimulation or supplementation. The fluorescence images were taken by an inverted fluorescence microscope (CKX53, Olympus Model) with digital camera (DP74, Olympus) and CellSens software Version 3.1.

Animal Study. *Animal Models for Kidney Failure and Vascular Calcification.* Vascular calcification was induced in 8 week old male Sprague−Dawley rats (initial weight of approximately 350 g) by feeding a diet containing adenine (0.75%), high levels of calcium (1.06%) and phosphate (0.92%), and a low level of protein (2.5%). The animals were fed for 4 weeks with this diet, followed by 2 weeks of feeding with a diet containing high calcium (1.06%) and phosphate (0.92%) only. The former and the latter diets are referred to as the adenine and CaP diets, respectively, hereafter. The adenine diet induces kidney failure due to the nephrotoxicity effects of adenine. This diet led to a significant weight loss, which was compensated by changing to a normal standard chow diet for 1−2 days when the weight loss was greater than 15%. Under the CaP diet, however, the rats did not have significant weight loss. The rats received humane care in compliance with the standard guidelines under Animal Ethic Application No. (2021/AE000409), approved by the anatomical bioscience ethics committee (ABS) at the University of Queensland.

Treatment with PSI NPs and Cur-PSI-OA NPs. The rats were acclimatized for 4 days and then divided into four groups of Control, PBS, PSI-OA NPs, and Cur-PSI-OA NPs treatments for the whole duration of study (6 weeks) (n = 8 rats/group). The treatment groups received 1 mL of dPBS solution, PSI-OA NPs, or Cur-PSI-OA NPs dispersed in dPBS through lateral tail vein intravenous (IV) injections. The dose was 50 mg of total NPs weight per kilogram of the rats' body weight. Such a dosage is equivalent to 2.15 mg of Cur/kg of the rat's weight, considering 86% encapsulation efficiency and Cur: PSI-OA mass ratio of 1:20 was used in the preparation. As shown in the timeline in Figure S1, the IV injections were conducted twice a week, from the second half of the first week until the end of the study (overall 11 injections). The animals in the Control group were sacrificed 4 days after delivery (for acclimatization purposes) without any injection or specific diet. At the end of the study, all the animals in the 3 remaining groups were euthanized by carbon dioxide asphyxiation, followed by immediate blood collection by cardiac puncture and organ collection.

Whole Aorta Staining with Alizarin Red S (ARS). From each group, 3 aortas were randomly assigned for ARS staining, while the rest were homogenized for calcium measurement, which will be discussed below. The whole aorta was placed in freshly prepared and filtered 2% ARS solution (pH 4.1−4.3) for 10 min and washed with DI water 3 times until there was a negligible red color in the water. The aortas were imaged by a stereomicroscope for qualitative detection of calcium deposits along the aortas.

Calcium Measurement in Aorta. The collected aortas were homogenized for 5 min in a lysis buffer with the following ingredients and final concentrations; Tris-HCl (20 mM), Triton X-100 (1%), SDS (0.1%), NaCl (50 mM), EDTA (2.5 mM), $Na_4P_2O_7{\cdot}10\ H_2O$ (1 mM), NaF (20 mM), Na_3VO_4 (1 mM), and protease inhibitor cocktail (Sigma, P8340) (1% (v/v)). The homogenized aortas were centrifuged at 10000g for 15 min. The supernatant was collected for Western blotting, while the pellet was dried for calcium measurement. The dried pellets were weighed and hydrolyzed by 1 mL of 6 M HCl at 80 °C for 4 h. The hydrolyzed pellets were dried, followed by reconstruction by 500 μL of 0.1 M HCl. The calcium content was measured colorimetrically with a calcium measurement kit (MAK022, Sigma) as mentioned above. The calculated calcium contents were normalized to the dry weight of aortas.

Histology of Organs. The collected organs, including heart, spleen, liver, kidneys, and aorta, were fixed in PFA 4% solution in dPBS. The fixed specimens were placed in plastic tissue processing cassettes and processed in a Tissue-Tek VIP^6 Tissue processor (Sakura, Olympus, Australia) on a 9 h protocol. Processed samples were embedded in paraffin using embedding console (Leica). Sections were cut at 4 μm using a Leica RM2235 paraffin microtome and collected on to ICON Printer Slides (InstrumeC, Australia). Slides were stained with hematoxylin and eosin (H&E) staining on a Tissue-Tek Prisma autostainer, and coverslipped on the attached Tissue-Tek- Glas automated Coverslipper (Sakura, Olympus, Australia). The aorta slides were also stained with freshly prepared Alizarin red S (2 wt %, pH 4.1−4.3) for detection of calcium deposits. Briefly, after deparaffinizing and hydrating with 70% ethanol, the slides were rinsed with DI water followed by 2 min of staining. The excess dye around the sections was gently removed with a tissue paper (kimwipe).

Blood Chemistry. The collected blood from the left ventricle puncture was left at room temperature for 30 min to clot and then centrifuged at 2000g for 15 min to separate the clot, followed by obtaining the serum. The collected serum was kept at −80 °C for later blood chemistry analysis. Calcium, phosphate, uric acid, blood urea nitrogen (BUN), and aspartate transaminase (AST) to alanine transaminase (ALT) ratio (AST/ALT) of the blood was measured.

Bone Integrity. After the animals were sacrificed, the femur was carefully removed from the hip joint and knee joint, and the surrounding soft tissue was removed gently. The bones were rinsed with PBS to remove debris and kept at 4 °C until test. The mechanical strength of the harvested femoral bones was measured using an Instron Model 3367 equipped with a 30 kN load cell under a three-point bending and circular geometry test modes. The support span and the extension rate were set at 20.5 mm and 1 mm/min, respectively. To measure the stress, the average diameters of the bones were obtained by measuring the diameter of at least 2 points in the middle where force is applied.

Statistical Analyses. Data are presented as mean ± SD from at least three independent experiments and analyzed with one- or two-way ANOVA. The statistical significance was defined as p-value < 0.05.

ASSOCIATED CONTENT

Supporting Information

The Supporting Information is available free of charge at https://pubs.acs.org/doi/10.1021/acsnano.3c03041.

(1) Schematic representation of the timeline of diet and intravenous injection (Figure S1); (2) analysis of the chemical structures of the synthesized polymers (Figure S2); (3) conjugation of PSI-OA NPs with different amine-containing molecules (Figure S3); (4) viability of MOVAS in the presence of PASP-OA an PSI-OA (Figure S4); (5) changes of AST and ALT in healthy rats and adenine-fed rats treated with different treatment (Figure S5); (6) size, PDI, and zeta potential results of the conjugation reaction between PSI-OA NP and FA-PEG-NH_2 (Table S1) (PDF)

AUTHOR INFORMATION

Corresponding Author

Hang Thu Ta − *Queensland Micro- and Nanotechnology Centre, Griffith University, Nathan, Queensland 4111, Australia; Australian Institute for Bioengineering and Nanotechnology, University of Queensland, St Lucia, Queensland 4072, Australia; Bioscience Discipline, School of Environment and Science, Griffith University, Nathan,*

https://doi.org/10.1021/acsnano.3c03041
ACS Nano 2023, 17, 18775−18791

Queensland 4111, Australia; orcid.org/0000-0003-1188-0472; Phone: +61 (7) 3735 5384; Email: h.ta@griffith.edu.au; https://hangta.group/

Authors

Hossein Adelnia − *Queensland Micro- and Nanotechnology Centre, Griffith University, Nathan, Queensland 4111, Australia; Australian Institute for Bioengineering and Nanotechnology, University of Queensland, St Lucia, Queensland 4072, Australia*

Shehzahdi Shebbrin Moonshi − *Queensland Micro- and Nanotechnology Centre, Griffith University, Nathan, Queensland 4111, Australia;* orcid.org/0000-0003-2048-595X

Yuao Wu − *Queensland Micro- and Nanotechnology Centre, Griffith University, Nathan, Queensland 4111, Australia*

Andrew C. Bulmer − *School of Pharmacy and Medical Sciences, Griffith University, Southport, Queensland 4222, Australia*

Ryan Mckinnon − *School of Pharmacy and Medical Sciences, Griffith University, Southport, Queensland 4222, Australia*

Jarred William Fastier-Wooller − *Department Precision Engineering, Graduate School of Engineering, The University of Tokyo, Tokyo 113-8656, Japan;* orcid.org/0000-0003-1119-2223

Idriss Blakey − *Australian Institute for Bioengineering and Nanotechnology, University of Queensland, St Lucia, Queensland 4072, Australia;* orcid.org/0000-0003-2389-6156

Complete contact information is available at: https://pubs.acs.org/10.1021/acsnano.3c03041

Notes

The authors declare no competing financial interest.

ACKNOWLEDGMENTS

This work is funded by National Health and Medical Research Council (HTT: APP1037310, APP1182347, APP2002827). H.A. is supported by a Ph.D. scholarship from University of Queensland. H.T.T. is supported by a Heart Foundation Future Fellowship (HTT: 102761). The authors would like to acknowledge the Australian National Fabrication Facility (Queensland Node) for access to key items of equipment.

REFERENCES

(1) Russo, D.; Corrao, S.; Battaglia, Y.; Andreucci, M.; Caiazza, A.; Carlomagno, A.; Lamberti, M.; Pezone, N.; Pota, A.; Russo, L.; et al. Progression of coronary artery calcification and cardiac events in patients with chronic renal disease not receiving dialysis. *Kidney Int.* **2011**, *80* (1), 112−118.

(2) Zia, A.; Wu, Y.; Nguyen, T.; Wang, X.; Peter, K.; Ta, H. T. The choice of targets and ligands for site-specific delivery of nanomedicine to atherosclerosis. *Cardiovasc. Res.* **2020**, *116* (13), 2055−2068.

(3) Wu, Y.; Vazquez-Prada, K. X.; Liu, Y.; Whittaker, A. K.; Zhang, R.; Ta, H. T. Recent Advances in the Development of Theranostic Nanoparticles for Cardiovascular Diseases. *Nanotheranostics* **2021**, *5* (4), 499−514.

(4) Nelson, A. J.; Raggi, P.; Wolf, M.; Gold, A. M.; Chertow, G. M.; Roe, M. T. Targeting vascular calcification in chronic kidney disease. *JACC Basic Transl Sci.* **2020**, *5* (4), 398−412.

(5) Leopold, J. A. Vascular calcification: mechanisms of vascular smooth muscle cell calcification. *Trends Cardiovasc. Med.* **2015**, *25* (4), 267−274.

(6) Neven, E.; D'Haese, P. C. Vascular calcification in chronic renal failure what have we learned from animal studies? *Circ. Res.* **2011**, *108* (2), 249−264.

(7) Himmelsbach, A.; Ciliox, C.; Goettsch, C. Cardiovascular calcification in chronic kidney disease-therapeutic opportunities. *Toxins (Basel)* **2020**, *12* (3), 181.

(8) Merlot, A. M.; Kalinowski, D. S.; Richardson, D. R. Novel chelators for cancer treatment: where are we now? *Antioxidants & Redox Signaling* **2013**, *18* (8), 973−1006.

(9) Wu, Y.; Ta, H. T. Different approaches to synthesising cerium oxide nanoparticles and their corresponding physical characteristics, and ROS scavenging and anti-inflammatory capabilities. *J. Mater. Chem. B* **2021**, *9* (36), 7291−7301.

(10) Wu, Y.; Cowin, G.; Moonshi, S. S.; Tran, H. D.; Fithri, N. A.; Whittaker, A. K.; Zhang, R.; Ta, H. T. Engineering chitosan nano-cocktail containing iron oxide and ceria: a two-in-one approach for treatment of inflammatory diseases and tracking of material delivery. *Materials Science and Engineering: C* **2021**, *131*, 112477.

(11) Tang, J. L.; Moonshi, S. S.; Ta, H. T. Nanoceria: an innovative strategy for cancer treatment. *Cell. Mol. Life Sci.* **2023**, *80* (2), 46.

(12) Perera, B.; Wu, Y.; Nguyen, N.-T.; Ta, H. T. Advances in drug delivery to atherosclerosis: Investigating the efficiency of different nanomaterials employed for different type of drugs. *Materials Today Bio* **2023**, *22*, 100767.

(13) Zhang, Y.; Koradia, A.; Kamato, D.; Popat, A.; Little, P. J.; Ta, H. T. Treatment of atherosclerotic plaque: perspectives on theranostics. *J. Pharm. Pharmacol* **2019**, *71* (7), 1029−1043.

(14) Torti, S. V.; Torti, F. M. Iron and cancer: more ore to be mined. *Nature reviews. Cancer* **2013**, *13* (5), 342−355.

(15) Demer, L. L.; Tintut, Y. Vascular Calcification. *Circulation* **2008**, *117* (22), 2938−2948.

(16) Adelnia, H.; Blakey, I.; Little, P. J.; Ta, H. T. Hydrogels based on poly(aspartic acid): synthesis and applications. *Frontiers in Chemistry* **2019**, *7*, 755.

(17) Adelnia, H.; Tran, H. D.; Little, P. J.; Blakey, I.; Ta, H. T. Poly (aspartic acid) in biomedical applications: From polymerization, modification, properties, degradation, and biocompatibility to applications. *ACS Biomaterials Science & Engineering* **2021**, *7* (6), 2083−2105.

(18) Adelnia, H.; Sirous, F.; Blakey, I.; Ta, H. T. Metal ion chelation of poly(aspartic acid): From scale inhibition to therapeutic potentials. *Int. J. Biol. Macromol.* **2023**, *229*, 974−993.

(19) Liu, T.; Wang, R.; Cao, H.; Lin, A. Polyaspartic acid alleviates heavy metal toxicity in zebrafish (Danio rerio). *Chemistry and Ecology* **2017**, *33* (7), 684−693.

(20) Wan, S.; Huang, J.; Guo, M.; Zhang, H.; Cao, Y.; Yan, H.; Liu, K. Biocompatible superparamagnetic iron oxide nanoparticle dispersions stabilized with poly (ethylene glycol)-oligo (aspartic acid) hybrids. *J. Biomed. Mater. Res., Part A* **2007**, *80A* (4), 946−954.

(21) Guo, S.; Ward, M. D.; Wesson, J. A. Direct visualization of calcium oxalate monohydrate crystallization and dissolution with atomic force microscopy and the role of polymeric additives. *Langmuir* **2002**, *18* (11), 4284−4291.

(22) Wesson, J.; Worcester, E. Formation of hydrated calcium oxalates in the presence of poly-L-aspartic acid. *Scanning microscopy* **1996**, *10* (2), 415-23−423-4.

(23) Rimer, J. D.; Kolbach-Mandel, A. M.; Ward, M. D.; Wesson, J. A. The role of macromolecules in the formation of kidney stones. *Urolithiasis* **2017**, *45* (1), 57−74.

(24) Sheng, X.; Ward, M. D.; Wesson, J. A. Adhesion between molecules and calcium oxalate crystals: critical interactions in kidney stone formation. *J. Am. Chem. Soc.* **2003**, *125* (10), 2854−2855.

(25) Adelnia, H.; Blakey, I.; Little, P. J.; Ta, H. T. Poly(succinimide) nanoparticles as reservoirs for spontaneous and sustained synthesis of poly(aspartic acid) under physiological conditions: potential for vascular calcification therapy and oral drug delivery. *J. Mater. Chem. B* **2023**, *11*, 2650−2662.

(26) Ray, S.; Adelnia, H.; Ta, H. T. Collagen and the effect of poly-l-lactic acid based materials on its synthesis. *Biomaterials Science* **2021**, *9* (17), 5714−5731.
(27) Sheng, H.; Zhou, J.; Li, B.; He, Y.; Zhang, X.; Liang, J.; Zhou, J.; Su, Q.; Xie, E.; Lan, W.; et al. A thin, deformable, high-performance supercapacitor implant that can be biodegraded and bioabsorbed within an animal body. *Science advances* **2021**, *7* (2), No. eabe3097.
(28) Zhang, R.; Zang, P.; Yang, D.; Li, J.; Hu, N.; Qu, S.; Yang, P. A Phase Engineering Strategy of Perovskite-Type ZnSnO3: Nd for Boosting the Sonodynamic Therapy Performance. *Adv. Funct. Mater.* **2023**, *33*, 2300522.
(29) Du, Y.; Zhang, R.; Yang, J.; Liu, S.; Zhou, J.; Zhao, R.; He, F.; Zhang, Y.; Yang, P.; Lin, J. A "closed-loop" therapeutic strategy based on mutually reinforced ferroptosis and immunotherapy. *Adv. Funct. Mater.* **2022**, *32* (13), 2111784.
(30) Croissant, J. G.; Fatieiev, Y.; Khashab, N. M. Degradability and clearance of silicon, organosilica, silsesquioxane, silica mixed oxide, and mesoporous silica nanoparticles. *Advanced materials* **2017**, *29* (9), 1604634.
(31) Chen, X.; Wu, Y.; Nguyen, N.-T.; Ta, H. T. Polymeric nanomaterial strategies to encapsulate and deliver biological drugs: points to consider between methods. *Biomaterials Science* **2023**, *11* (6), 1923−1947.
(32) Li, H.; Sureda, A.; Devkota, H. P.; Pittalà, V.; Barreca, D.; Silva, A. S.; Tewari, D.; Xu, S.; Nabavi, S. M. Curcumin, the golden spice in treating cardiovascular diseases. *Biotechnology Advances* **2020**, *38*, 107343.
(33) Giordano, A.; Tommonaro, G. Curcumin and cancer. *Nutrients* **2019**, *11* (10), 2376.
(34) Hanna, D. H.; Saad, G. R. Nanocurcumin: preparation, characterization and cytotoxic effects towards human laryngeal cancer cells. *RSC Adv.* **2020**, *10* (35), 20724−20737.
(35) Anwer, M. K.; Al-Shdefat, R.; Ezzeldin, E.; Alshahrani, S. M.; Alshetaili, A. S.; Iqbal, M. Preparation, evaluation and bioavailability studies of eudragit coated PLGA nanoparticles for sustained release of eluxadoline for the treatment of irritable bowel syndrome. *Frontiers in pharmacology* **2017**, *8*, 844.
(36) Wong, C. Y.; Al-Salami, H.; Dass, C. R. Microparticles, microcapsules and microspheres: a review of recent developments and prospects for oral delivery of insulin. *International journal of pharmaceutics* **2018**, *537* (1−2), 223−244.
(37) Adelnia, H.; Ensandoost, R.; Moonshi, S. S.; Gavgani, J. N.; Vasafi, E. I.; Ta, H. T. Freeze/thawed polyvinyl alcohol hydrogels: present, past and future. *Eur. Polym. J.* **2022**, *164*, 110974.
(38) Salakhieva, D. V.; Gumerova, D.; Akhmadishina, R.; Kamalov, M.; Nizamov, I.; Nemeth, C.; Szilágyi, A.; Abdullin, T. Anti-radical and cytotoxic activity of polysuccinimide and polyaspartic acid of different molecular weight. *BioNanoScience* **2016**, *6* (4), 348−351.
(39) Juriga, D. v.; Nagy, K.; Jedlovszky-Hajdú, A. l.; Perczel-Kovách, K.; Chen, Y. M.; Varga, G. b.; Zrínyi, M. s. Biodegradation and osteosarcoma cell cultivation on poly (aspartic acid) based hydrogels. *ACS Appl. Mater. Interfaces* **2016**, *8* (36), 23463−23476.
(40) Kuhn, D. A.; Vanhecke, D.; Michen, B.; Blank, F.; Gehr, P.; Petri-Fink, A.; Rothen-Rutishauser, B. Different endocytotic uptake mechanisms for nanoparticles in epithelial cells and macrophages. *Beilstein journal of nanotechnology* **2014**, *5* (1), 1625−1636.
(41) Low, P. S.; Henne, W. A.; Doorneweerd, D. D. Discovery and development of folic-acid-based receptor targeting for imaging and therapy of cancer and inflammatory diseases. *Accounts of chemical research* **2008**, *41* (1), 120−129.
(42) Poh, S.; Chelvam, V.; Ayala-López, W.; Putt, K. S.; Low, P. S. Selective liposome targeting of folate receptor positive immune cells in inflammatory diseases. *Nanomedicine: Nanotechnology, Biology and Medicine* **2018**, *14* (3), 1033−1043.
(43) Low, P. S.; Antony, A. C. Folate receptor-targeted drugs for cancer and inflammatory diseases. *Advanced drug delivery reviews* **2004**, *56* (8), 1055−1058.
(44) Jahandideh, A.; Uotila, S.; Ståhle, M.; Virta, J.; Li, X.-G.; Kytö, V.; Marjamäki, P.; Liljenbäck, H.; Taimen, P.; Oikonen, V.; et al. Folate receptor β-targeted PET Imaging of macrophages in autoimmune myocarditis. *J. Nucl. Med.* **2020**, *61* (11), 1643−1649.
(45) Ayubi, M.; Karimi, M.; Abdpour, S.; Rostamizadeh, K.; Parsa, M.; Zamani, M.; Saedi, A. Magnetic nanoparticles decorated with PEGylated curcumin as dual targeted drug delivery: Synthesis, toxicity and biocompatibility study. *Materials Science and Engineering: C* **2019**, *104*, 109810.
(46) Gholibegloo, E.; Mortezazadeh, T.; Salehian, F.; Ramazani, A.; Amanlou, M.; Khoobi, M. Improved curcumin loading, release, solubility and toxicity by tuning the molar ratio of cross-linker to β-cyclodextrin. *Carbohydr. Polym.* **2019**, *213*, 70−78.
(47) Skafi, N.; Abdallah, D.; Soulage, C.; Reibel, S.; Vitale, N.; Hamade, E.; Faour, W.; Magne, D.; Badran, B.; Hussein, N.; et al. Phospholipase D: A new mediator during high phosphate-induced vascular calcification associated with chronic kidney disease. *Journal of cellular physiology* **2019**, *234* (4), 4825−4839.
(48) Mackenzie, N.; Zhu, D.; Longley, L.; Patterson, C.; Kommareddy, S.; MacRae, V. MOVAS-1 cell line: a new in vitro model of vascular calcification. *International journal of molecular medicine* **2011**, *27* (5), 663−668.
(49) Li, X.-Y.; Li, Q.-M.; Fang, Q.; Zha, X.-Q.; Pan, L.-H.; Luo, J.-P. Laminaria japonica polysaccharide inhibits vascular calcification via preventing osteoblastic differentiation of vascular smooth muscle cells. *Journal of agricultural and food chemistry* **2018**, *66* (8), 1821−1827.
(50) Neven, E.; d'Haese, P. C. Vascular calcification in chronic renal failure: what have we learned from animal studies? *Circulation research* **2011**, *108* (2), 249−264.
(51) Price, P.; Roublick, A.; Williamson, M. Artery calcification in uremic rats is increased by a low protein diet and prevented by treatment with ibandronate. *Kidney international* **2006**, *70* (9), 1577−1583.
(52) Diwan, V.; Brown, L.; Gobe, G. C. Adenine-induced chronic kidney disease in rats. *Nephrology* **2018**, *23* (1), 5−11.
(53) Diwan, V.; Mistry, A.; Gobe, G.; Brown, L. Adenine-induced chronic kidney and cardiovascular damage in rats. *Journal of pharmacological and toxicological methods* **2013**, *68* (2), 197−207.
(54) Matsui, I.; Hamano, T.; Mikami, S.; Fujii, N.; Takabatake, Y.; Nagasawa, Y.; Kawada, N.; Ito, T.; Rakugi, H.; Imai, E. Fully phosphorylated fetuin-A forms a mineral complex in the serum of rats with adenine-induced renal failure. *Kidney international* **2009**, *75* (9), 915−928.
(55) Karamched, S. R.; Nosoudi, N.; Moreland, H. E.; Chowdhury, A.; Vyavahare, N. R. Site-specific chelation therapy with EDTA-loaded albumin nanoparticles reverses arterial calcification in a rat model of chronic kidney disease. *Sci. Rep.* **2019**, *9* (1), 2629.
(56) Choi, H. K.; Liu, S.; Curhan, G. Intake of purine-rich foods, protein, and dairy products and relationship to serum levels of uric acid: the Third National Health and Nutrition Examination Survey. *Arthritis & Rheumatism: Official Journal of the American College of Rheumatology* **2005**, *52* (1), 283−289.
(57) Henley, C.; Davis, J.; Miller, G.; Shatzen, E.; Cattley, R.; Li, X.; Martin, D.; Yao, W.; Lane, N.; Shalhoub, V. The calcimimetic AMG 641 abrogates parathyroid hyperplasia, bone and vascular calcification abnormalities in uremic rats. *European journal of pharmacology* **2009**, *616* (1−3), 306−313.
(58) Adirekkiat, S.; Sumethkul, V.; Ingsathit, A.; Domrongkitchaiporn, S.; Phakdeekitcharoen, B.; Kantachuvesiri, S.; Kitiyakara, C.; Klyprayong, P.; Disthabanchong, S. Sodium thiosulfate delays the progression of coronary artery calcification in haemodialysis patients. *Nephrology Dialysis Transplantation* **2010**, *25* (6), 1923−1929.
(59) Rotman, S. G.; Moriarty, T. F.; Nottelet, B.; Grijpma, D. W.; Eglin, D.; Guillaume, O. Poly(aspartic acid) functionalized poly(ϵ-caprolactone) microspheres with enhanced hydroxyapatite affinity as bone targeting antibiotic carriers. *Pharmaceutics* **2020**, *12* (9), 885.
(60) Lotsari, A.; Rajasekharan, A. K.; Halvarsson, M.; Andersson, M. Transformation of amorphous calcium phosphate to bone-like apatite. *Nat. Commun.* **2018**, *9* (1), 4170.

https://doi.org/10.1021/acsnano.3c03041
ACS Nano 2023, 17, 18775−18791

(61) Fu, Y.-C.; Fu, T.-F.; Wang, H.-J.; Lin, C.-W.; Lee, G.-H.; Wu, S.-C.; Wang, C.-K. Aspartic acid-based modified PLGA-PEG nanoparticles for bone targeting: In vitro and in vivo evaluation. *Acta biomaterialia* **2014**, *10* (11), 4583−4596.
(62) Jiang, T.; Yu, X.; Carbone, E. J.; Nelson, C.; Kan, H. M.; Lo, K. W.-H. Poly aspartic acid peptide-linked PLGA based nanoscale particles: potential for bone-targeting drug delivery applications. *International journal of pharmaceutics* **2014**, *475* (1−2), 547−557.
(63) Fisher, S.; Burgess, W. L.; Hines, K. D.; Mason, G. L.; Owiny, J. R. Interstrain differences in CO2-induced pulmonary hemorrhage in mice. *Journal of the American Association for Laboratory Animal Science* **2016**, *55* (6), 811−815.
(64) Danneman, P. J.; Stein, S.; Walshaw, S. O. Humane and practical implications of using carbon dioxide mixed with oxygen for anesthesia or euthanasia of rats. *Laboratory Animal Science* **1997**, *47* (4), 376−385.
(65) Klinkhammer, B. M.; Djudjaj, S.; Kunter, U.; Palsson, R.; Edvardsson, V. O.; Wiech, T.; Thorsteinsdottir, M.; Hardarson, S.; Foresto-Neto, O.; Mulay, S. R.; et al. Cellular and molecular mechanisms of kidney injury in 2, 8-dihydroxyadenine nephropathy. *Journal of the American Society of Nephrology* **2020**, *31* (4), 799−816.
(66) Opdebeeck, B.; Neven, E.; Millán, J. L.; Pinkerton, A. B.; D'Haese, P. C.; Verhulst, A. Chronic kidney disease-induced arterial media calcification in rats prevented by tissue non-specific alkaline phosphatase substrate supplementation rather than inhibition of the enzyme. *Pharmaceutics* **2021**, *13* (8), 1138.
(67) Tomida, M.; Nakato, T.; Matsunami, S.; Kakuchi, T. Convenient synthesis of high molecular weight poly (succinimide) by acid-catalysed polycondensation of L-aspartic acid. *J. Polym. Sci., Part A: Polym. Chem.* **1997**, *38* (18), 4733−4736.
(68) Gyenes, T.; Torma, V.; Gyarmati, B.; Zrínyi, M. Synthesis and swelling properties of novel pH-sensitive poly (aspartic acid) gels. *Acta biomaterialia* **2008**, *4* (3), 733−744.
(69) Liu, Y.; Wu, Y.; Zhang, R.; Lam, J.; Ng, J. C.; Xu, Z.-P.; Li, L.; Ta, H. T. Investigating the use of layered double hydroxide nanoparticles as carriers of metal oxides for theranostics of ROS-related diseases. *ACS Applied Bio Materials* **2019**, *2*, 5930−5940.
(70) Wu, Y.; Yang, Y.; Zhao, W.; Xu, Z. P.; Little, P. J.; Whittaker, A. K.; Zhang, R.; Ta, H. T. Novel iron oxide-cerium oxide core-shell nanoparticles as a potential theranostic material for ROS related inflammatory diseases. *J. Mater. Chem. B* **2018**, *6* (30), 4937−4951.
(71) Wu, Y.; Zhang, R.; Tran, H. D.; Kurniawan, N. D.; Moonshi, S. S.; Whittaker, A. K.; Ta, H. T. Chitosan nanococktails containing both ceria and superparamagnetic iron oxide nanoparticles for reactive oxygen species-related theranostics. *ACS Applied Nano Materials* **2021**, *4* (4), 3604−3618.
(72) Rehman, A. U.; Wu, Y.; Tran, H. D.; Vazquez-Prada, K.; Liu, Y.; Adelnia, H.; Kurniawan, N. D.; Anjum, M. N.; Moonshi, S. S.; Ta, H. T. Silver/iron oxide nano-popcorns for imaging and therapy. *ACS Applied Nano Materials* **2021**, *4* (10), 10136−10147.

https://doi.org/10.1021/acsnano.3c03041
ACS Nano 2023, 17, 18775−18791

Supporting Information for

A Bioactive Disintegrable Polymer Nanoparticle for Synergistic Vascular Anti-Calcification

Hossein Adelnia[1,2], Shehzahdi Shebbrin Moonshi[1], Yuao Wu[1], Andrew C. Bulmer[4], Ryan Mckinnon[4], Jarred William Fastier-Wooller[5], Idriss Blakey[2], Hang Thu Ta[1,2,3,*]

[1] Queensland Micro-and Nanotechnology Centre, Griffith University, Nathan, Queensland 4111, Australia

[2] Australian Institute for Bioengineering and Nanotechnology, University of Queensland, St Lucia, Queensland 4072, Australia

[3] Bioscience Discipline, School of Environment and Science, Griffith University, Nathan, Queensland 4111, Australia.

[4] School of Pharmacy and Medical Sciences, Griffith University, Southport, Queensland 4222, Australia

[5] Department Precision Engineering, Graduate School of Engineering, The University of Tokyo, Tokyo 113-8656, Japan

*Correspondence: Hang Thu Ta (h.ta@griffith.edu.au)

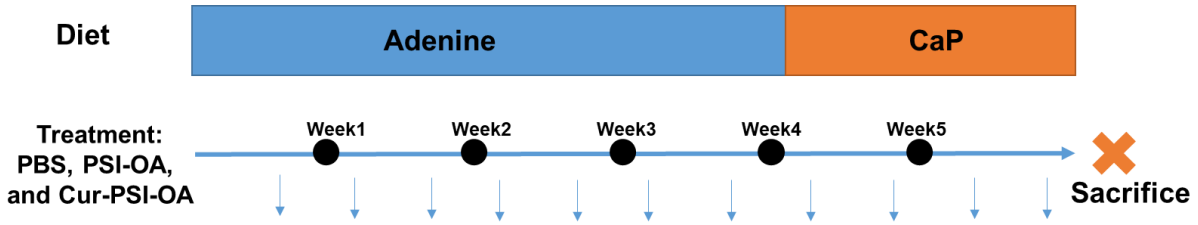

Fig S1: Schematic representation of the timeline of diet and i.v. injections.

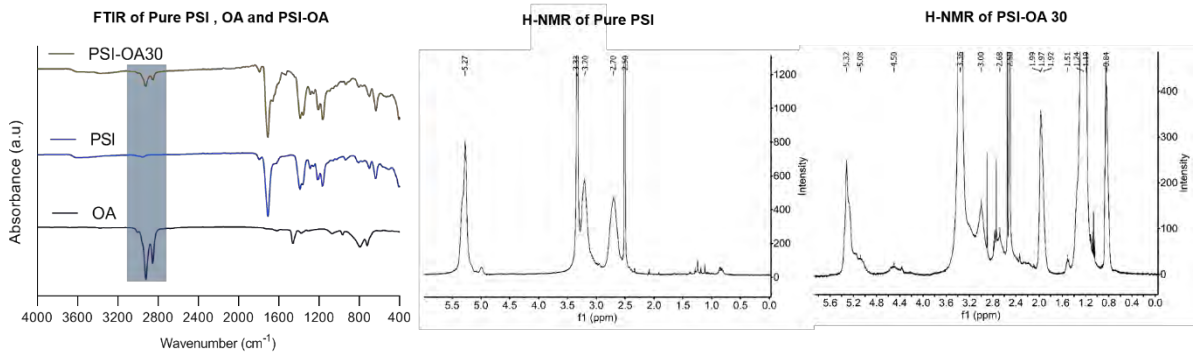

Fig. S2. Analysis of the chemical structures of the synthesized polymers. FTIR of pure OA, pure PSI, and PSI-OA. H-NMR of pure PSI, and PSI-OA30 in d6-DMSO. The characteristic peaks of PSI are seen at δ (in ppm) values of 2.70, 3.21, 5.27. The characteristic peaks of PSI-OA are seen at δ (in ppm) values of 0.85, 1.20, 1.23, 1.26, 1.51, 1.92, 1.97, 2.68, 3.00, 3.36, 4.49, 5.08, 5.32.

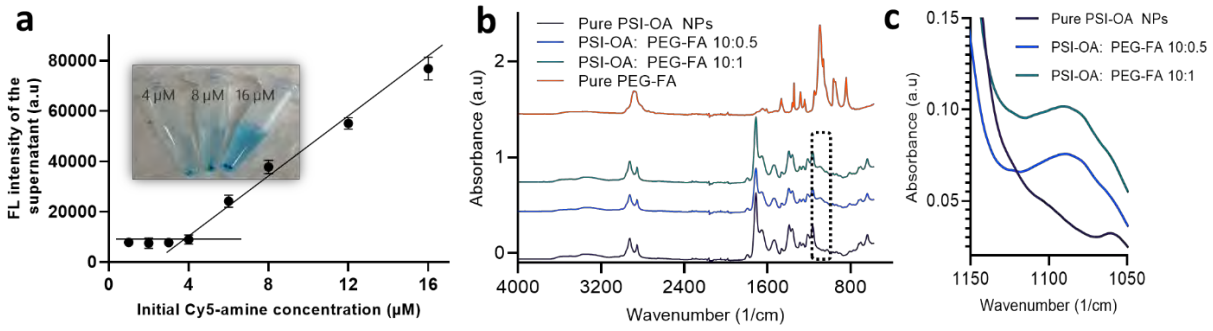

Fig. S3. Conjugation of PSI-OA NPs with different amine-containing molecules. (a) Fluorescence intensity of the supernatant at different concentrations of Cy5-amine in the reaction. **(b)** ATR-FTIR spectra of pure PSI-OA NP, pure PEG-FA, and conjugated NPs at different ratios of 10:0.5, and 10:1. The characteristic peak of PEG is at 1088cm^{-1}, which is seen in the conjugated NPs when the spectra are magnified **(c)** (right ATR-FTIR panel).

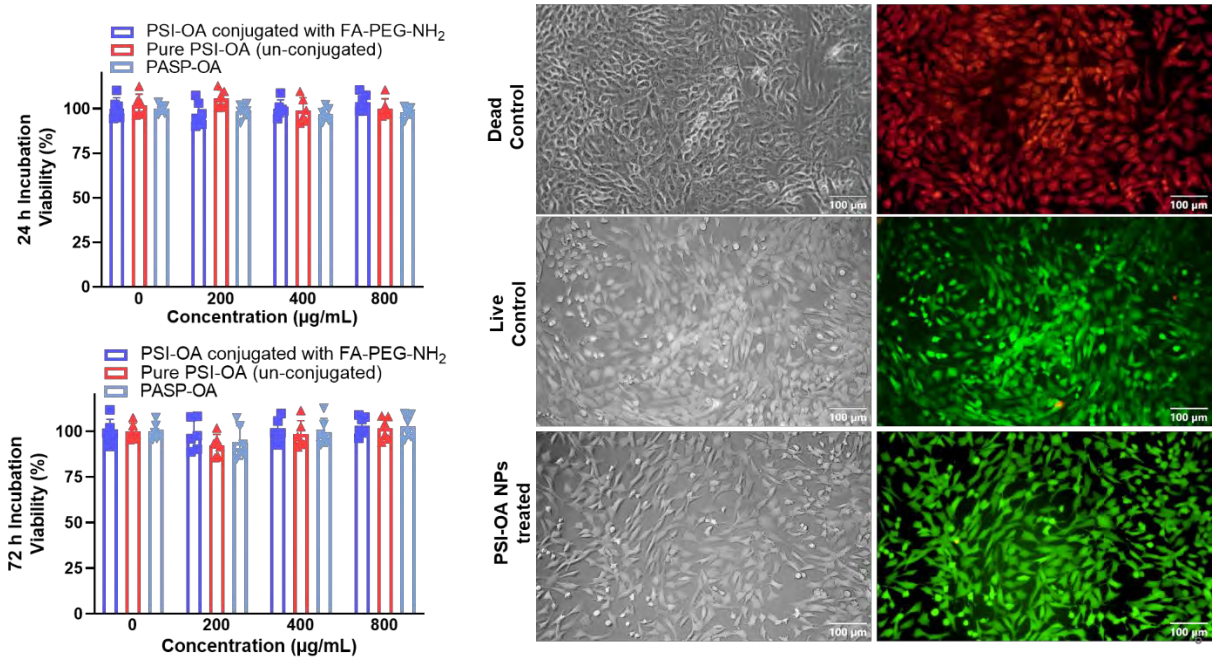

Fig. S4. Viability of MOVAS in the presence of different concentration of PASP-OA as well as PSI-OA (with and without conjugation with FA-PEG-NH$_2$). The results are the average of 3 values for PrestoBlue assay and no significant difference was found at the tested concentrations at both 24 and 72 h incubation. The comparison was carried out with respect to cell control (0 µg/mL). The right panel shows Live/Dead cell assay where green and red respectively indicate live and dead cells. As seen, the FA-PEG-conjugated PSI-OA treated MOVAS after 3 days incubation at concentration of 800 µg/mL, shows no significant red color, further verifying the biocompatibility of the NPs. The scale bar is 100 µm.

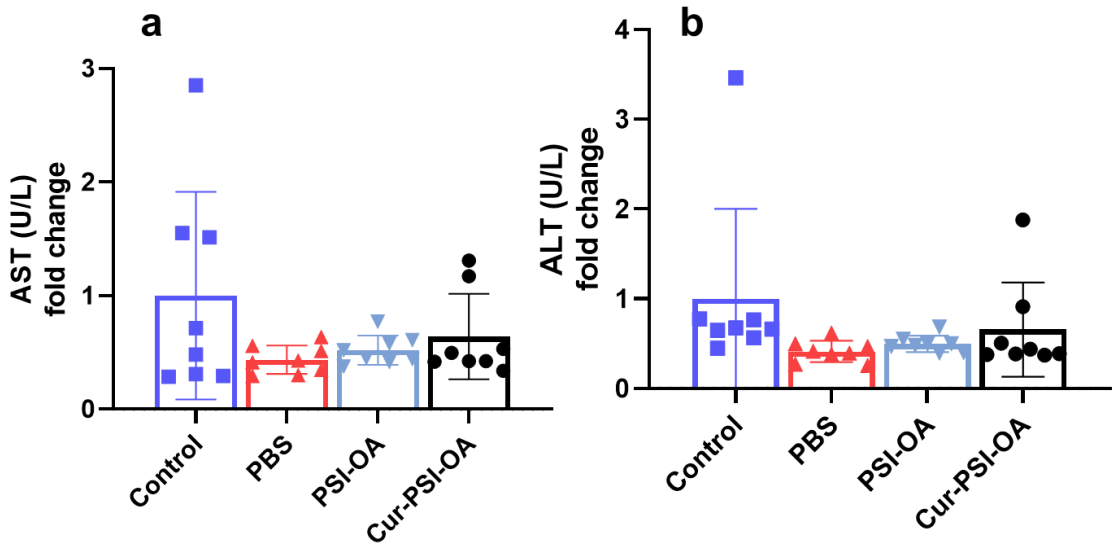

Fig. S5. (a) AST, and (b) ALT fold changes in healthy rats and adenine-fed rats treated with PBS or PSI-OA and Cur-PSI-OA.

Table 1. Size, PDI, and zeta potential results of the conjugation reaction between PSI-OA NP and FA-PEG-NH_2

Sample	Size (nm)	PDI (%)	Zeta potential in DI water (mV)
Pure PSI-OA NPs	188	5.4	-19
FA:NP 1:10	182	17	-10
FA:NP 2:10	196	11.6	-18
FA:NP 5:10	194	1.2	-17.5